

# Predissociation rates in carbon monoxide: dependence on rotational state, parity and isotope

K.S.E. Eikema, W. Hogervorst and W. Ubachs

*Laser Centre, Department of Physics and Astronomy, Vrije Universiteit, De Boelelaan 1081,  
1081 HV Amsterdam, The Netherlands*

Received 30 August 1993

A high-resolution spectroscopic study of carbon monoxide has been performed using a narrow-band and tunable extreme-ultraviolet laser source in the wavelength range 91–97 nm. For three isotopes  $^{12}\text{C}^{16}\text{O}$ ,  $^{13}\text{C}^{16}\text{O}$  and  $^{13}\text{C}^{18}\text{O}$  the  $(4p\pi)\text{L}^1\Pi$ ,  $v=0$ ,  $(4p\sigma)\text{K}^1\Sigma^+$ ,  $v=0$  and  $(3s\sigma)\text{W}^1\Pi$ ,  $v=0$  states were investigated. The  $^1\Pi$ ,  $v=2$ ,  $(3s\sigma)\text{W}^1\Pi$ ,  $v=2$  and  $(3d\pi)\text{L}'^1\Pi$ ,  $v=1$  states were studied for  $^{12}\text{C}^{16}\text{O}$  and  $^{13}\text{C}^{16}\text{O}$ . The  $^1\Pi$ ,  $v=0$  state at  $109564.58\text{ cm}^{-1}$ , the  $(6p\sigma)^1\Sigma^+$ ,  $v=0$  state at  $109173.68\text{ cm}^{-1}$ , the  $(5p\sigma)^1\Sigma^+$ ,  $v=0$  state at  $107174.44\text{ cm}^{-1}$ , and the  $(4d\sigma)^1\Sigma^+$ ,  $v=0$  state at  $105676.30\text{ cm}^{-1}$  were excited only for the main isotope  $^{12}\text{C}^{16}\text{O}$ . Previously unknown states are found at  $107365.87\text{ cm}^{-1}$  ( $^1\Sigma^+$ ) for  $^{12}\text{C}^{16}\text{O}$  and at  $103203.07\text{ cm}^{-1}$  ( $^1\Pi$ ) for  $^{13}\text{C}^{18}\text{O}$ . Indirect evidence is found for a perturber state at  $107708 \pm 2\text{ cm}^{-1}$  for  $^{12}\text{C}^{16}\text{O}$ , while spectroscopic information on the  $\text{E}^1\Pi$ ,  $v=5$  state of  $^{13}\text{C}^{18}\text{O}$  is deduced from a deperturbation analysis. A rotational-state and isotope-dependent predissociation rate is found for almost all states. A parity dependence is observed for the  $(4p\pi)\text{L}^1\Pi$ ,  $v=0$  and  $(3s\sigma)\text{W}^1\Pi$ ,  $v=0$  states, where the predissociation rate of the  $\Pi$ , component varies proportional to  $J(J+1)$ . This effect is attributed to a coupling with the repulsive part of the  $\text{D}'^1\Sigma^+$  state. Several examples of accidental predissociations have been found, particularly in the  $(4d\sigma)^1\Sigma^+$ ,  $v=0$  state.

## 1. Introduction

Considerable progress in the extreme-ultraviolet (XUV) spectroscopy of molecular hydrogen [1] and carbon monoxide [2–9] has been reported in recent years. Of these two most widespread molecular species in the interstellar medium CO is readily observable by radioastronomy and for this reason it is commonly used as a tracer molecule in searches for and detailed analyses of interstellar clouds. Absorption and radiative transfer in the XUV spectral range and XUV-induced photodissociation processes are known to largely influence the chemical dynamics of the interstellar medium [10–13]. In particular photodissociation at short wavelengths, manifesting itself through predissociation of bound Rydberg states, is the dominant loss process of CO in dense molecular clouds. As photodestruction takes place via discrete line absorption rather than through continuum absorption [2], accurate spectroscopic information on the highly excited states of CO, including the absorption and dissociation rates, is required. For the interior of dense clouds the Prasad–Tarafdar model in-

volving cosmic-ray-induced XUV photons may play a role [13]. Here the precise determination of coincidences between  $\text{H}_2$  emission lines and CO absorption lines in the XUV range is requested. A long-standing problem is that of the C/CO ratio in the interstellar medium, which is found to be much larger than predicted by steady-state models [14]. The relative over-abundance of carbon atoms may be explained assuming additional photodestruction processes of CO [15] or by revision of the photodissociation rates. A motivation for the continuing efforts devoted to spectroscopic studies of the high-lying states of CO, like the present one, is the desire to find answers to the aforementioned questions.

Isotope effects are found to be of major importance. Because the purely rotational transitions of the main  $^{12}\text{C}^{16}\text{O}$  isotopomer are often saturated microwave spectra of the less-abundant species, such as  $^{13}\text{C}^{16}\text{O}$ ,  $^{12}\text{C}^{18}\text{O}$  and  $^{13}\text{C}^{18}\text{O}$ , are also recorded in radioastronomical searches. In fact these rare isotopomers are primarily used to map cloud density distributions. The ratio  $^{12}\text{C}/^{13}\text{C}$  or  $^{16}\text{O}/^{18}\text{O}$  is found to

vary over the different molecular species [11,16]. Isotopic fractionation in XUV-induced photodissociation may occur in case of large isotope shifts of the predissociating states. This isotopic fractionation depends on the optical depth inside interstellar clouds considering also self-shielding effects in XUV absorption. In the model of van Dishoeck and Black [10] the  $E^1\Pi-X^1\Sigma^+$  (1,0) and  $W^1\Pi-X^1\Sigma^+$  (2,0) bands were e.g. found to be most effective in the isotope-selective photodissociation. Isotopic fractionation may also be caused by isotope-dependent predissociation rates, but these effects are not yet incorporated in the complex models. Some strong isotope effects were observed by the Meudon group [3,4] in their comprehensive study of CO in the range 91–115 nm. They found that the  $J(4s\sigma)^1\Sigma^+-X^1\Sigma^+$  (0,0) band at 98.56 nm broadened into a diffuse pattern by predissociation for  $^{12}\text{C}^{16}\text{O}$ , while the spectra for  $^{13}\text{C}^{16}\text{O}$ ,  $^{12}\text{C}^{18}\text{O}$  and  $^{13}\text{C}^{18}\text{O}$  were rotationally resolved. For the  $(4d\sigma)^1\Sigma^+-X^1\Sigma^+$  (0,0) band at 94.63 nm the opposite is the case; it is diffuse except for  $^{12}\text{C}^{16}\text{O}$ .

In previous studies we reported on the use of an XUV laser source for accurate measurements of predissociation linewidths in vibronic bands of CO [6,7]. From natural samples weak spectra of  $^{13}\text{C}^{16}\text{O}$  could be recorded as well and an isotope effect of a factor of two was found for the predissociation rate of the  $W^1\Pi, v=2$  state. In the present investigation these isotope effects were studied in more detail using a  $^{13}\text{C}$  enriched sample. Moreover, due to an improved detection efficiency, resulting in a tenfold increase in signal-to-noise ratio, also rotational state and  $A$ -doublet dependencies of predissociation rates could now be deduced. Recently in an elegant two-laser fluorescence-dip experiment Drabbels et al. [8] observed such effects. Their data are highly accurate, but predissociation rates could only be deduced for states with  $J \leq 4$  ( $J$  is the total angular momentum). In the present study the analysis of rotational-state and  $A$ -doublet dependency of predissociation was extended to higher  $J$ -values, in some cases as high as  $J=25$ , to other vibronic states and to other isotopic species than  $^{12}\text{C}^{16}\text{O}$ . The recording of a large rotational manifold introduces new complexities in the analysis. E.g. the  $(4d\sigma)^1\Sigma^+, v=0$  state is found to interact with at least three different dissociative perturber states at higher  $J$ -values. The  $K(4p\sigma)^1\Sigma^+, v=0$

state of  $^{13}\text{C}^{18}\text{O}$  is found to be perturbed for  $J \geq 5$  and from a detailed analysis the perturber state could be tentatively assigned to be  $E^1\Pi, v=5$ . In the following details will be presented on the rotational structure and predissociation effects of the  $^1\Pi, v=0$  {7A} state, the  $(6p\sigma)^1\Sigma^+, v=0$  {8B} state, a  $^1\Pi, v=2$  {13} state, a complex manifold of systems in the interval 93.1–93.3 nm {15A–B–C}, the  $W(3s\sigma)^1\Pi, v=2$  {18} and  $v=0$  {28} states, the  $(4d\sigma)^1\Sigma^+, v=0$  {19} state, the  $L(4p\pi)^1\Pi, v=0$  {25} state, the  $L'(3d\pi)^1\Pi, v=1$  {26} state and the  $K(4p\sigma)^1\Sigma^+, v=0$  {27} state. The numbers in curly brackets { } refer to the initial numbering of the Meudon group [2–4] and will be used throughout this paper. In addition two new states are found: one at  $107365.87 \text{ cm}^{-1}$  ( $^1\Sigma^+$ ) for  $^{12}\text{C}^{16}\text{O}$  and at  $103203.07 \text{ cm}^{-1}$  ( $^1\Pi$ ) for  $^{13}\text{C}^{18}\text{O}$ .

## 2. Experiment

A description of the XUV laser spectrometer has been presented in several previous publications [6,7,17]. Basically the setup consists of a crossed laser/molecular beam configuration for sub-Doppler resolution. XUV radiation is generated by frequency tripling UV pulses (4 ns) from a frequency-doubled pulsed dye laser in a pulsed jet of xenon or acetylene gas, depending on the specific wavelength. XUV and UV beams are temporally and spatially overlapped. A scheme of the experimental arrangement is shown in fig. 1.

The CO spectra were recorded by employing the technique of 1 XUV + 1 UV photoionization in combination with time-of-flight (TOF) mass selection.  $^{12}\text{C}^{16}\text{O}$  spectra were obtained from measurements on a natural CO sample, using a dense pulsed beam and averaging over up to 20 laser pulses per frequency setting. By varying time delay settings and stagnation pressure cold ( $\approx 40 \text{ K}$ ) as well as near-room-temperature population distributions over rotational states could be prepared in the molecular beam. The state distribution is not always Boltzmann-like. In particular at higher temperatures the distribution in the beam does not correspond to a single well-defined temperature. Nevertheless, the approximate temperature control of the molecular beam greatly facilitated the assignment of  $J$ -states.

A  $^{13}\text{C}$  enriched sample of 1 bar-liter containing

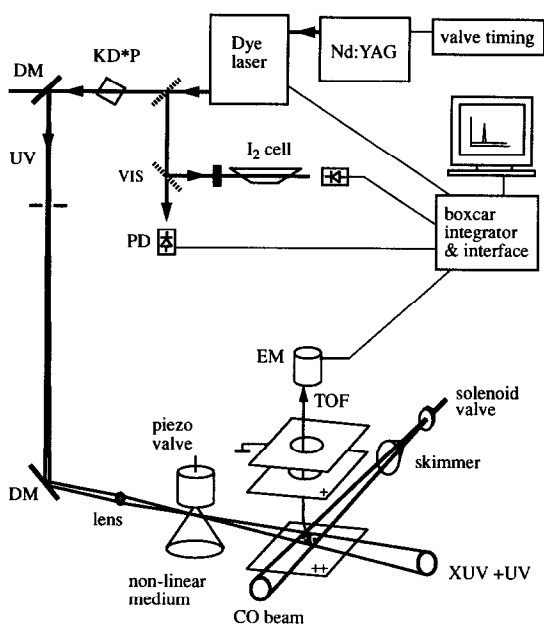


Fig. 1. The experimental setup. The solenoid valve for CO gas pulses, the piezo-electrically-driven valve for the tripling gas, and the interaction region are in three separated differentially pumped vacuum chambers. KD\*P is the crystal for frequency doubling. DM are dichroic mirrors. EM is the electron multiplier for the detection of ions.

about 10%  $^{13}\text{C}^{18}\text{O}$  mixed in  $^{13}\text{C}^{16}\text{O}$  was available. With the use of the TOF mass selector and two boxcar integrators independent spectra of  $^{13}\text{C}^{16}\text{O}$  and  $^{13}\text{C}^{18}\text{O}$  could be recorded simultaneously. However, at those frequency positions, where  $^{13}\text{C}^{16}\text{O}$  signals were strong, the spectra of  $^{13}\text{C}^{18}\text{O}$  were contaminated by  $^{13}\text{C}^{16}\text{O}$  signals. Because of the limited quantity of the  $^{13}\text{C}$ -enriched sample a compromise was sought between molecular beam density, the number of pulses used for signal averaging, the number of recordings and the specific bands to be recorded. In well-planned sessions, lasting in total for 12 hours, the isotopic bands of  $^{13}\text{CO}$  presented in this work could be recorded. In total about 400000 molecular beam pulses were counted with the laser system running at 10 Hz and a sample of 1 bar-liter.

In the experimental setup, which is basically the same as in previous studies on CO [6,7], several improvements were made that resulted in an increase of the signal-to-noise ratio of more than an order of magnitude. This was accomplished by reducing the

background ion signal in two ways. Firstly, the diffusion pumps of two differentially pumped vacuum chambers were refilled with Santovac oil, that has a lower UV-induced ionization cross section. Secondly, UV stray light was kept from exposing the capacitor plates, which are used for the extraction of resonant signal ions. This largely reduced a strong non-resonant ion signal at the CO mass. The improved signal-to-noise ratio allowed for the extraction of more detailed information on line shapes from the spectra.

As the XUV radiation is obtained by frequency sextupling a tunable dye laser in the visible an accurate calibration of the XUV transition frequencies against the  $\text{I}_2$  standard is possible [18,19]. XUV spectra were recorded simultaneously with  $\text{I}_2$  spectra and stored on a SUN-4 computer. The absolute accuracy in the CO line positions is estimated to be  $0.13 \text{ cm}^{-1}$  [7]. For the broadened or weak lines the uncertainty is larger and may amount to  $0.3 \text{ cm}^{-1}$ . Previously an instrument-limited linewidth of  $0.32 \pm 0.06 \text{ cm}^{-1}$  was reported, predominantly caused by the bandwidth of the dye laser ( $\approx 0.07 \text{ cm}^{-1}$ ). A contribution of the residual Doppler width of  $< 0.02 \text{ cm}^{-1}$  is contained in this value. In the meantime a detailed investigation of the instrumental linewidth of the XUV-laser spectrometer was performed by recording and analyzing several transitions in  $\text{N}_2$  in the wavelength interval 90.5–95 nm [17]. The width was found to vary linearly from  $0.44 \text{ cm}^{-1}$  at 90.5 nm to  $0.32 \text{ cm}^{-1}$  at 95 nm with a typical uncertainty of 10%. This effect closely follows a variation in the bandwidth of the dye laser providing the fundamental wavelength.

Predissociation rates of excited states are determined from broadening effects of the CO lines. The observed line profiles are fitted to Voigt functions from which a width  $\delta\nu_{\text{obs}}$  is deduced. For a derivation of the natural linewidth  $\Gamma$  (in  $\text{cm}^{-1}$ ) an analytical deconvolution formula was used [20]:

$$\Gamma = \delta\nu_{\text{obs}} - \frac{(\delta\nu_{\text{instr}})^2}{\delta\nu_{\text{obs}}}, \quad (1)$$

which is valid if the instrumental line profile is a Gaussian lineshape.  $\Gamma$  corresponds to a Lorentzian. In the study on  $\text{N}_2$  [17] it was verified that indeed the instrumental line profile is approximately Gaussian. The wavelength-dependent instrumental line-

width  $\delta\nu_{\text{instr}}$  in the interval 90.5–95 nm was interpolated in between 0.44 and 0.32  $\text{cm}^{-1}$ . For  $\lambda > 95$  nm the values were extrapolated linearly. Indeed the lines of the  $L(4p\pi) \ ^1\Pi-X \ ^1\Sigma^+$  (0,0) band at 96.8 nm with the lowest  $J$ -values showed spectral widths of 0.30  $\text{cm}^{-1}$ , corresponding to this extrapolated value.

Predissociation rate  $k_p$ , lifetime  $\tau$ , and natural linewidth  $\Gamma$  (in  $\text{cm}^{-1}$ ) are related by

$$k_p = \frac{1}{\tau} = 2\pi\Gamma c, \quad (2)$$

assuming radiative relaxation to be a much slower process than predissociation [2,3]. Then excited state lifetimes and predissociation rates can be derived straightforwardly from linewidth measurements. We estimate that from lines recorded with reasonable signal-to-noise a lifetime broadening effect as small as 30% of the instrumental width can be deduced without ambiguity. After deconvolution with eq. (1) this corresponds to  $\Gamma \approx 0.15 \text{ cm}^{-1}$ . The maximum lifetime that can be measured is then  $\tau \approx 3 \times 10^{-11} \text{ s}$ , corresponding to a minimum predissociation rate of  $k_p \approx 3 \times 10^{10} \text{ s}^{-1}$ .

Additional information on relative predissociation rates is comprised in the line intensities. In the Appendix a relationship between signal intensities in the process of 1 XUV + 1 UV photoionization and lifetimes of the excited states is derived in terms of a rate equation model. In the domain where the laser linewidth  $\delta\nu_{\text{Laser}}$  exceeds the natural width  $\Gamma$  a proportionality relation is found:

$$I_{\text{signal}} \propto \tau, \quad \text{for } \Gamma \ll \delta\nu_{\text{Laser}}, \quad (3)$$

whereas in the case of the large broadening we obtain

$$I_{\text{signal}} \propto \tau^2, \quad \text{for } \Gamma \gg \delta\nu_{\text{Laser}}. \quad (4)$$

In the intermediate regime the signal intensity depends on the lifetime through the following relation:

$$I_{\text{signal}} \propto \tau^\alpha, \quad \text{for } \Gamma \approx \delta\nu_{\text{Laser}}, \quad (5)$$

with  $1 < \alpha < 2$  and  $\alpha$  dependent on  $(\Gamma/\delta\nu_{\text{Laser}})$ . In the latter case no quantitative conclusions will be drawn, although in a qualitative sense the signal intensities still provide information on the relative lifetimes of the excited states. We remark that in eqs. (3)–(5) it is assumed that XUV intensity and ionization cross sections for the 1 XUV + 1 UV two-photon-ionization process are constant; for rotational states within

a certain vibronic manifold these assumptions are likely to be valid. Eqs. (3)–(5) have the consequence that excited states with a lifetime on the order of  $3 \times 10^{-12} \text{ s}$  or less cannot be observed in the present setup because of intensity loss. For this reason states such as  $H(4p\sigma) \ ^1\Sigma^+, v=1 \{21\}$  could not be observed, and no attempt was even made to record  $^{13}\text{CO}$  spectra of the  $(4d\sigma) \ ^1\Sigma^+, v=0 \{19\}$  state, knowing it to be diffuse in the study of Eidelsberg and Rostas [3].

### 3. Results

XUV excitation spectra of a selected number of bands were recorded in the wavelength range 91.6–97.3 nm. An attempt was made to reexamine in high resolution all vibronic states listed in the interval 91–98 nm by the Meudon group [2–4]. Nine states were investigated using the XUV-laser source in a previous study [7]. Transitions to some of these states are reinvestigated in the present work with a much higher signal-to-noise ratio, thus revealing greater detail. With the improved setup four other vibronic states for the main isotope  $^{12}\text{C}^{16}\text{O}$  could be observed. The rotational structure of the bands was analysed using energy expressions for the excited states:

$$E_{\Sigma}(J) = \nu_0 + BJ(J+1) - DJ^2(J+1)^2 \quad (6)$$

in the case of a  $^1\Sigma^+$  state and

$$E_{\Pi_c}(J) = \nu_0 + BJ(J+1) - DJ^2(J+1)^2 + qJ(J+1), \quad (7)$$

$$E_{\Pi_r}(J) = \nu_0 + BJ(J+1) - DJ^2(J+1)^2 \quad (8)$$

in the case of a  $^1\Pi$  state. Here  $\nu_0$  is the band origin (energy above the  $X \ ^1\Sigma^+, v=0, J=0$  ground state),  $B$  the rotational constant,  $D$  the centrifugal distortion constant and  $q$  the  $A$ -doubling parameter.  $\Pi_c$  levels are probed in P and R transitions, while the  $\Pi_r$  levels are probed in the Q branch. Ground state rotational levels were calculated from the spectroscopic constants of Guelachvili et al. [21]. Molecular constants for the excited states were derived in least squares minimization routines for each specific state. In the fitting procedures not all data points were given identical weights. Overlapped, weak or broadened lines were accredited lower weights. Also use was made of

low and higher temperature molecular beams for the disentanglement of low  $J$ - and high  $J$ -state contributions. Molecular constants and uncertainties resulting from the fits are listed in table 1. For most of the bands the number of lines observed is less than in the study of the Meudon group [2–4], particularly when intensities were low and only a cold molecular beam could be used. As a consequence in these cases the improved absolute accuracy of line positions did not result in more accurate values for  $B$  and  $D$  constants. Then the values of the Meudon group were used and fixed in the minimization routines, thus yielding an accurate value for the band origins.

In those cases where the rotational structure was found to be irregular, a deperturbation analysis for the excited state was performed. Deperturbed energies for the observed state  $E_{\text{obs}}(J)$  and for a perturber manifold  $E_{\text{pert}}(J)$  are then expressed in terms of eqs. (6)–(8). Perturbed energies are then found by diagonalizing a matrix for each  $J$  [22]:

$$\begin{pmatrix} E_{\text{obs}}(J) & H_{\text{int}} \\ H_{\text{int}} & E_{\text{pert}}(J) \end{pmatrix}, \quad (9)$$

where  $H_{\text{int}}$  represents an interaction matrix element. Phenomenologically a distinction is made between homogeneous and heterogeneous interactions. For a homogeneous perturbation the interaction matrix element

$$H_{\text{int}} = H_{\text{hom}} \quad (10)$$

is independent of  $J$ . For a heterogeneous perturbation the interaction matrix element is rotational-state dependent. It may be shown that in the latter case the  $J$ -dependence is [22]

$$H_{\text{int}} = H_{\text{het}} \sqrt{J(J+1) - \Omega(\Omega+1)}, \quad (11)$$

with  $\Omega$  the projection of the electronic angular momentum on the internuclear axis of the molecule. For couplings between a  ${}^1\Sigma^+$  state and a  ${}^1\Pi$  state the interaction matrix element is then

$$H_{\text{int}} = H_{\text{het}} \sqrt{J(J+1)}, \quad (12)$$

while for a coupling between a  ${}^1\Pi$  state and a  ${}^1\Delta$  state

$$H_{\text{int}} = H_{\text{het}} \sqrt{J(J+1) - 2} \quad (13)$$

is found. Heterogeneous perturbations are found between states of different electronic symmetry, whereas homogeneous perturbations mostly occur between

states of equal electronic symmetry, although a spin-orbit interaction between states of different electronic symmetry may also give rise to a homogeneous perturbation [22]. In practice, when the character of the perturber state is not a priori known, both perturbation analyses are followed, and it may well be that one of the two results in a more accurate description of the observed state [23]. This then provides a handle to assign the perturber state.

### 3.1. The ${}^1\Pi, v=0$ state {7A}

An XUV excitation spectrum of the  ${}^1\Pi, v=0$  state {7A} of  ${}^{12}\text{C}^{16}\text{O}$  recorded at  $\lambda=91.27$  nm is presented in fig. 2. Also shown is the simultaneously recorded  $I_2$  absorption spectrum used for the calibration of line positions in the XUV. The weak CO spectrum, which could not be observed in the previous study because of poor signal-to-noise, was obtained from a high-density cold expansion and by averaging over 20 pulses per frequency setting. Only a few low  $J$ -values were observed. The P(2) line, the lowest  $J$ -value in the P branch, is expected to be weaker than the R(2) line because of a smaller Hönl–London factor. For this reason it is not surprising that the whole P branch is missing at the present level of signal-to-noise ratio. Derived line positions are listed in table 2. The spectral width observed is  $0.44 \text{ cm}^{-1}$ , averaging over several recordings and all  $J$ -states. The regular intensity pattern (following an approximate Boltzmann distribution at 40 K) indicates that there is no rotational effect on the lifetime. The value of  $0.44 \text{ cm}^{-1}$  corresponds, within error limits, to the instrumental line-width at 91.2 nm and a predissociation rate  $k_p < 3 \times 10^{10} \text{ s}^{-1}$  is estimated for the  ${}^1\Pi, v=0$  state {7A}. Because of the low intensity in this band no spectra of  ${}^{13}\text{CO}$  were recorded.

### 3.2. The $(6p\sigma) {}^1\Sigma^+, v=0$ state {8B}

A rather weak excitation spectrum of the  $(6p\sigma) {}^1\Sigma^+, v=0$  {8B} Rydberg state at  $\lambda=91.6$  nm, recorded again under the conditions of a high-density cold expansion of pure CO, is shown in fig. 3. The intensity pattern is regular, in agreement with a low-temperature population distribution. The line-width is determined by averaging over all lines, yielding  $0.45 \pm 0.05 \text{ cm}^{-1}$ . Again this corresponds, within

Table 1

Molecular constants for excited states of CO as obtained from least squares fits. A spectroscopic assignment of the states is given as well as the numbering in curly brackets { } following refs. [2-4]. For comparison the  $B$ -constants of ref. [3] are also given. A new value for the  $D$ -constant is only given when a more accurate value than that in ref. [3] is found. The quoted error in the value for  $\nu_0$  represents the relative uncertainty from the fit; the estimated absolute accuracy is 0.13  $\text{cm}^{-1}$ . All values are in  $\text{cm}^{-1}$ .

| State                          | $\nu_0$          | $B$             | $B$ (ref. [3])  | $D$                              | $q$                               |
|--------------------------------|------------------|-----------------|-----------------|----------------------------------|-----------------------------------|
| $^{12}\text{C}^{16}\text{O}$   |                  |                 |                 |                                  |                                   |
| $^1\Pi, \nu=0$                 | 109564.58 ± 0.07 | 1.915 ± 0.004   | 1.9226 ± 0.0035 | 5.9 × 10 <sup>-5 a)</sup>        |                                   |
| $6pc\ ^1\Sigma^+, \nu=0$       | 109173.68 ± 0.06 | 1.684 ± 0.005   | 1.716 ± 0.042   | 1.0 × 10 <sup>-4 a)</sup>        |                                   |
| $^1\Pi, \nu=2$ (homogeneous)   | 107682.33 ± 0.06 | 1.936 ± 0.001   | 1.9118 ± 0.003  | 7 × 10 <sup>-6 a)</sup>          |                                   |
| perturber state                | 107706 ± 1       | 1.64 ± 0.02     |                 |                                  |                                   |
| $^1\Pi, \nu=2$ (heterogeneous) | 107681.95 ± 0.08 | 1.936 ± 0.001   |                 | (3.1 ± 0.3) × 10 <sup>-5</sup>   |                                   |
| perturber state                | 107710.1 ± 0.8   | 1.604 ± 0.005   |                 |                                  |                                   |
| $5pc\ ^1\Sigma^+, \nu=0$       | 107174.44 ± 0.05 | 2.24 ± 0.02     | 2.128 ± 0.011   | 1.0 × 10 <sup>-5 a)</sup>        |                                   |
| $^1\Sigma^+$                   | 107365.87 ± 0.04 | 1.884 ± 0.004   |                 | (3.1 ± 0.9) × 10 <sup>-4</sup>   |                                   |
| $3scw\ ^1\Pi, \nu=2$           | 106250.90 ± 0.05 | 1.6224 ± 0.0004 | 1.6260 ± 0.0027 | (-1.3 ± 0.6) × 10 <sup>-5</sup>  | (-2.7 ± 0.5) × 10 <sup>-3</sup>   |
| $4dc\ ^1\Sigma^+, \nu=0$       | 105676.30 ± 0.04 | 1.8952 ± 0.0002 | 1.8829 ± 0.0021 | (1.73 ± 0.04) × 10 <sup>-5</sup> |                                   |
| $4prL\ ^1\Pi, \nu=0$           | 103271.84 ± 0.03 | 1.9599 ± 0.0002 | 1.9796 ± 0.0018 | (6.5 ± 0.9) × 10 <sup>-6</sup>   | (2.13 ± 0.03) × 10 <sup>-2</sup>  |
| $4pcK\ ^1\Sigma^+, \nu=0$      | 103054.71 ± 0.02 | 1.9159 ± 0.0002 | 1.9166 ± 0.0003 | (5.85 ± 0.06) × 10 <sup>-5</sup> |                                   |
| $3scw\ ^1\Pi, \nu=0$           | 102806.74 ± 0.03 | 1.564 ± 0.001   | 1.5622 ± 0.0003 | (8.5 ± 0.4) × 10 <sup>-5</sup>   |                                   |
| $^{13}\text{C}^{16}\text{O}$   |                  |                 |                 |                                  |                                   |
| $^1\Pi, \nu=2$                 | 107593.47 ± 0.03 | 1.850 ± 0.001   | 1.8496 ± 0.0006 | 7 × 10 <sup>-6 a)</sup>          |                                   |
| $3scw\ ^1\Pi, \nu=2$           | 106196.42 ± 0.06 | 1.5542 ± 0.002  | 1.5370 ± 0.0026 | (-1.4 ± 1.0) × 10 <sup>-4</sup>  | (-5.0 ± 0.8) × 10 <sup>-3</sup>   |
| $4prL\ ^1\Pi, \nu=0$           | 103248.85 ± 0.02 | 1.8922 ± 0.0002 |                 | (7.9 ± 0.1) × 10 <sup>-5</sup>   |                                   |
| $3drL\ ^1\Pi, \nu=1$           | 103161.3 ± 0.1   | 1.69 ± 0.01     |                 | 1.0 × 10 <sup>-5 a)</sup>        |                                   |
| $K\ ^1\Sigma^+, \nu=0$         | 103054.41 ± 0.03 | 1.8308 ± 0.0006 | 1.8174 ± 0.0036 | (1.02 ± 0.02) × 10 <sup>-4</sup> |                                   |
| $3scw\ ^1\Pi, \nu=0$           | 102775.77 ± 0.02 | 1.5019 ± 0.0003 | 1.5016 ± 0.0046 | (8.9 ± 0.3) × 10 <sup>-5</sup>   | (1.5 ± 0.7) × 10 <sup>-3</sup>    |
| $^{13}\text{C}^{18}\text{O}$   |                  |                 |                 |                                  |                                   |
| $4prL\ ^1\Pi, \nu=0$           | 103262.45 ± 0.04 | 1.759 ± 0.001   |                 | 1.0 × 10 <sup>-5 a)</sup>        |                                   |
| $^1\Pi$                        | 103203.07 ± 0.03 | 1.7082 ± 0.0003 |                 | 1.0 × 10 <sup>-5 a)</sup>        | (-1.51 ± 0.07) × 10 <sup>-2</sup> |
| $K\ ^1\Sigma^+, \nu=0$         | 103054.02 ± 0.04 | 1.7477 ± 0.0002 |                 | (1.43 ± 0.03) × 10 <sup>-5</sup> |                                   |
| $E\ ^1\Pi, \nu=5$              | 103073.44 ± 0.15 | 1.507 ± 0.002   |                 | (2.3 ± 0.2) × 10 <sup>-5</sup>   |                                   |
| $3scw\ ^1\Pi, \nu=0$           | 102743.26 ± 0.03 | 1.4313 ± 0.0006 |                 | (2.0 ± 0.5) × 10 <sup>-5</sup>   | (2.0 ± 0.5) × 10 <sup>-3</sup>    |

a) Parameter kept fixed in the minimization routine.

b) Homogeneous perturbation analysis with  $H_{\text{hom}} = 3.03 \pm 0.07\ \text{cm}^{-1}$ .

c) Heterogeneous perturbation analysis with  $H_{\text{het}} = 0.35 \pm 0.02\ \text{cm}^{-1}$ .

d) Heterogeneous perturbation analysis with  $H_{\text{het}} = 1.018 \pm 0.003\ \text{cm}^{-1}$ .

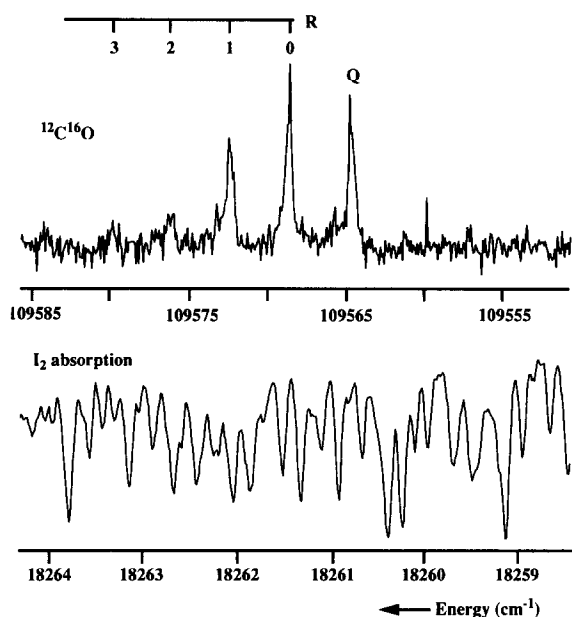


Fig. 2. XUV excitation spectrum of the transition to the  ${}^1\Pi, \nu=0$  state {7A} of  ${}^{12}\text{C}^{16}\text{O}$  at  $\lambda=91.27$  nm. Below, the simultaneously recorded absorption spectrum of  $\text{I}_2$  used for calibration purposes is shown.

Table 2  
Observed and calculated line positions (in  $\text{cm}^{-1}$ ) of the  ${}^1\Pi, \nu=0$ - $\text{X}^1\Sigma^+, \nu=0$  transition {7A} for  ${}^{12}\text{C}^{16}\text{O}$  at  $\lambda=91.27$  nm

| $J$ | $R(J)$    | Obs. - calc. | $Q(J)$    | Obs. - calc. |
|-----|-----------|--------------|-----------|--------------|
| 0   | 109568.43 | 0.02         |           |              |
| 1   | 109572.25 | 0.03         | 109564.50 | -0.06        |
| 2   | 109576.05 | 0.04         |           |              |
| 3   | 109579.76 | -0.03        |           |              |

error limits, to the instrument-limited linewidth. So no effect of lifetime broadening can be discerned and the predissociation rate is estimated  $k_p < 3 \times 10^{10} \text{ s}^{-1}$ . The regular intensity pattern again indicates that a possible predissociation is rotational-state independent. Observed line positions are listed in table 3.

### 3.3. The ${}^1\Pi, \nu=2$ state {9A}

At 91.73 nm a red-shaded band consisting of partly overlapping lines was observed. The signal intensity was barely above the noise level, and hence a detailed rotational analysis was not possible. The spectrum

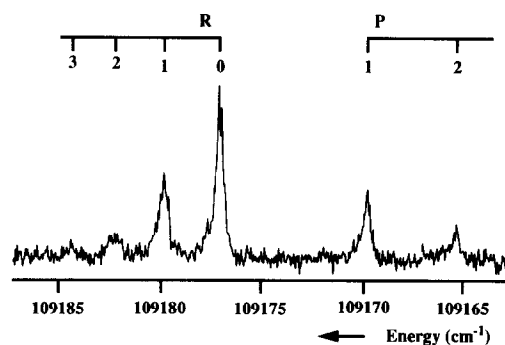


Fig. 3. Recording of the  $(6p\sigma) {}^1\Sigma^+ - \text{X}^1\Sigma^+ (0,0)$  band {8B} of  ${}^{12}\text{C}^{16}\text{O}$  at  $\lambda=91.60$  nm.

Table 3  
Observed and calculated line positions (in  $\text{cm}^{-1}$ ) of the  $6p\sigma {}^1\Sigma^+, \nu=0$ - $\text{X}^1\Sigma^+, \nu=0$  transition {8B} of  ${}^{12}\text{C}^{16}\text{O}$  at  $\lambda=91.60$  nm

| $J$ | $R(J)$    | Obs. - calc. | $P(J)$    | Obs. - calc. |
|-----|-----------|--------------|-----------|--------------|
| 0   | 109177.12 | 0.07         |           |              |
| 1   | 109179.89 | -0.05        | 109169.91 | 0.08         |
| 2   | 109182.26 | -0.09        | 109165.45 | -0.06        |
| 3   | 109184.35 | 0.08         | 109160.69 | -0.02        |

appeared to be diffuse and we estimate a spectral width of  $2.6 \pm 0.5 \text{ cm}^{-1}$ . This results in a large predissociation rate  $k_p = 5 \pm 1 \times 10^{11} \text{ s}^{-1}$ . This state was observed before in absorption by Eidelsberg and Rostas [3] and a relatively large integrated absorption cross section was determined. The weak intensity presently observed in 1+1 photoionization is consistent with the large predissociation rate (see eqs. (3)–(5) and Appendix).

### 3.4. The ${}^1\Pi, \nu=2$ state {13}

Strong excitation spectra of the  ${}^1\Pi, \nu=2$  state {13} of  ${}^{12}\text{C}^{16}\text{O}$  and  ${}^{13}\text{C}^{16}\text{O}$ , recorded at 92.86 and 92.94 nm respectively, are presented in fig. 4. The reproducible feature indicated with (?) nearly coinciding with the P(7) line of  ${}^{12}\text{C}^{16}\text{O}$  is not identified. Because it has no counterpart in the R branch, in which the same states are probed as in the P branch, the feature is not related to the  ${}^1\Pi, \nu=2$  state. A single separate line is not likely to be of molecular origin. However, it is measured from a pure CO beam and detected at mass 28. A possible explanation might be

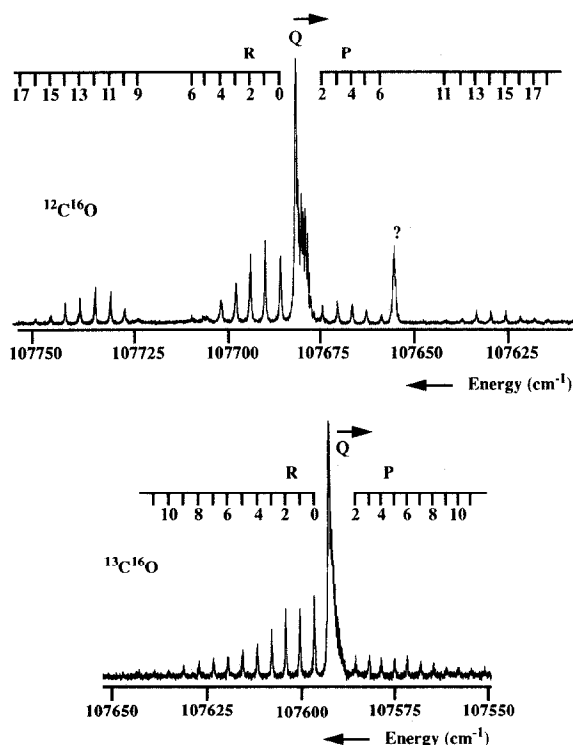


Fig. 4. The transitions to the  $^1\Pi, v=2$  state {13} for  $^{12}\text{C}^{16}\text{O}$  (upper) and  $^{13}\text{C}^{16}\text{O}$  (lower) at 92.87 nm and 92.94 nm resp. The feature marked with (?) is probably not related to CO (see text).

that the feature is related to doubly ionized iron ( $\text{Fe}^{2+}$ ) with mass 56, somehow produced in the interaction region. Carbon monoxide is known to be often contaminated by metal-hexacarbonyl molecules.

A clear perturbation is found in the spectrum of  $^{12}\text{C}^{16}\text{O}$  at  $J=8-9$  in the excited state. Near  $J=5, 6$  and  $J=10, 11$  a distinct line-broadening effect is observed, whereas the transitions to  $J=8$  and  $9$  have disappeared. The broadening is accompanied by a loss of intensity as expected in case of predissociation. Similarly in the  $^{13}\text{C}^{16}\text{O}$  spectrum the lines for  $J \geq 5$  in the excited states tend to broaden as well. Here the line intensities for  $J \geq 5$  decrease faster than expected on grounds of population, but consistent with a predissociation effect. Although the Q-branch lines are not resolved, apart from a few high  $J$  lines in the  $^{12}\text{C}^{16}\text{O}$  spectrum, nevertheless a clear intensity drop is observed in the  $^{12}\text{C}^{16}\text{O}$  spectrum at the location

where  $J=8$  and  $9$  are expected. The Q branch of  $^{13}\text{C}^{16}\text{O}$  follows the same pattern as the P and R branch: a monotonic decrease towards higher  $J$ -states. From these trends we conclude that there is a rotational-state dependence, but no  $A$ -doublet dependence, of the predissociation rates of the  $^1\Pi, v=2$  state.

The linewidths were fitted to Voigt profiles and deconvoluted from an estimated instrumental linewidth of  $0.42 \text{ cm}^{-1}$  at the excitation wavelength. Rotational-state-dependent predissociation rates could be determined. Values obtained for R and P transitions are averaged and plotted as a function of  $J$  (excited-state total angular momentum quantum number) in fig. 5. For  $^{12}\text{C}^{16}\text{O}$  a predissociation resonance is found at  $J=8-9$ , a clear indication of an accidental resonance. As a consequence the perturber must be a bound state, that predissociates however extremely rapidly. The perturbation manifests itself also in the form of an anti-crossing located in between  $J=8$  and  $9$ . When the level energies of  $\Pi_e(J)$  are fitted to a simple rotor model, according to eq. (7), states with  $J \leq 8$  are shifted downward in energy and states with  $J \geq 9$  upward. Such a perturbation may be induced by an interacting vibronic state with a larger value for  $\nu_0$  and a smaller  $B$ -constant. From the fact that the perturbation is found for the  $\Pi_f(J)$  levels as well (dip in

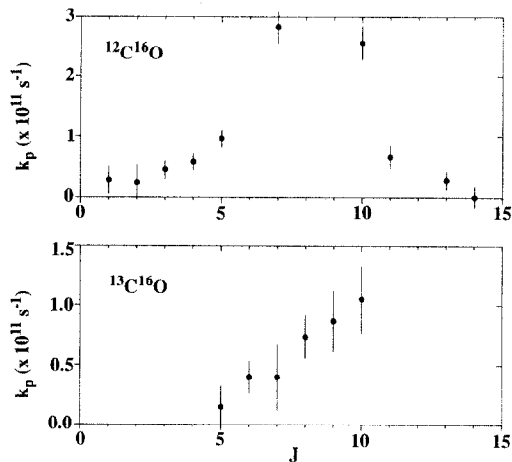


Fig. 5. Rotational-state-dependent predissociation rates for the  $\Pi_e$  components in  $^1\Pi, v=2, J$ -states {13} for  $^{12}\text{C}^{16}\text{O}$  (upper) and  $^{13}\text{C}^{16}\text{O}$  (lower). The data are derived from linewidths in the P and R branches. The  $\Pi_f$  components appear to have the same predissociation rates (see text).

the Q branch) it follows that the perturber state is definitely not a  $\Sigma^+$  or a  $\Sigma^-$  state, as these would affect only one parity component of the  ${}^1\Pi$  state.

The transition frequencies of P and R lines, listed in table 4, of the locally perturbed spectrum of  ${}^{12}\text{C}^{16}\text{O}$  were treated in a deperturbation analysis, using a  $J$ -dependent as well as a constant interaction parameter. In both procedures the observed data fit remarkably well with a standard deviation of  $0.05\text{ cm}^{-1}$ . In table 4 the differences between observed and calculated energies are included. The two models yield no significant difference for the calculated line positions. The presence of a local predissociating perturber is firmly established but its electronic symmetry cannot be stated unambiguously. The outcome of the deperturbation procedure is unequivocal, so no definite values of deperturbed molecular constants can be given. For this reason two sets of molecular parameters for this  ${}^1\Pi, \nu=2$  state as well as for the perturber state are included in table 1. Two possible assignments for the perturber can be given: either a  ${}^1\Delta$  state with a band origin at  $107710.1\text{ (8) cm}^{-1}$  or a  ${}^1\Pi$  state with a band origin at  $107706\text{ (1) cm}^{-1}$ .

For  ${}^{13}\text{C}^{16}\text{O}$  the predissociation rate linearly increases for states with  $J \geq 5$ . Here no discernable effect on the transition frequencies is found. The line positions are listed in table 5. In principle the mechanism causing the predissociation of the  ${}^{13}\text{C}^{16}\text{O}$  iso-

Table 5

Observed and calculated line positions (in  $\text{cm}^{-1}$ ) of the  ${}^1\Pi, \nu=2-X\ {}^1\Sigma^+, \nu=0$  transition {13} of  ${}^{13}\text{C}^{16}\text{O}$  at  $\lambda=92.94\text{ nm}$

| $J$ | $R(J)$    | Obs. – calc. | $P(J)$    | Obs. – calc. |
|-----|-----------|--------------|-----------|--------------|
| 0   | 107597.13 | –0.05        |           |              |
| 1   | 107600.88 | –0.02        |           |              |
| 2   | 107604.71 | 0.06         | 107586.22 | 0.07         |
| 3   | 107608.44 | 0.02         | 107582.55 | 0.03         |
| 4   | 107612.23 | 0.02         | 107578.88 | –0.04        |
| 5   | 107616.60 | 0.03         | 107575.21 | –0.13        |
| 6   | 107619.91 | 0.04         | 107571.78 | –0.00        |
| 7   | 107623.70 | –0.03        | 107568.20 | –0.05        |
| 8   | 107627.51 | –0.11        | 107564.80 | 0.05         |
| 9   | 107631.54 | 0.01         | 107561.30 | 0.03         |
| 10  | 107635.40 | –0.06        | 107558.02 | 0.21         |
| 11  | 107639.25 | –0.17        | 107554.59 | 0.20         |
| 12  | 107643.56 | 0.15         | 107550.88 | –0.11        |

tope may differ from that in  ${}^{12}\text{C}^{16}\text{O}$ . E.g. a rotational predissociation mechanism associated with a tunnelling process may explain the increase of the predissociation rate for  $J \geq 5$ . However, it is likely that the predissociation mechanisms for  ${}^{12}\text{C}^{16}\text{O}$  and  ${}^{13}\text{C}^{16}\text{O}$  are identical, and that in  ${}^{13}\text{C}^{16}\text{O}$  a local perturbation occurs at  $J > 10$ . The expected intensity revival across the anti-crossing is, however, not observed, due to a low level of signal-to-noise at  $J > 15$ . If the assumption of a local perturber is valid its band

Table 4

Observed and calculated line positions (in  $\text{cm}^{-1}$ ) of the  ${}^1\Pi, \nu=2-X\ {}^1\Sigma^+, \nu=0$  transition {13} of  ${}^{12}\text{C}^{16}\text{O}$  at  $\lambda=92.86\text{ nm}$

| $J$ | $R(J)$    | Obs. – calc. | $A_{\text{pert}}$ | $P(J)$    | Obs. – calc. | $A_{\text{pert}}$ |
|-----|-----------|--------------|-------------------|-----------|--------------|-------------------|
| 0   | 107685.80 | –0.01        | –0.01             |           |              |                   |
| 1   | 107689.75 | 0.06         | 0.06              |           |              |                   |
| 2   | 107693.60 | 0.02         | 0.02              | 107674.20 | –0.08        | –0.07             |
| 3   | 107697.43 | –0.04        | –0.06             | 107670.47 | 0.00         | 0.01              |
| 4   | 107701.27 | –0.07        | –0.15             | 107666.71 | 0.04         | 0.04              |
| 5   | 107705.31 | 0.14         | –0.05             | 107662.88 | 0.01         | –0.01             |
| 6   | 107708.79 | –0.06        | –0.53             | 107659.04 | –0.02        | –0.08             |
| 9   | 107722.94 | 0.00         | 1.68              |           |              |                   |
| 10  | 107726.53 | 0.02         | 1.26              |           |              |                   |
| 11  | 107730.19 | –0.09        | 0.91              | 107642.26 | 0.01         | 1.68              |
| 12  | 107734.05 | –0.08        | 0.75              | 107638.14 | –0.00        | 1.24              |
| 13  | 107737.98 | 0.00         | 0.65              | 107634.32 | 0.07         | 1.07              |
| 14  | 107741.86 | 0.05         | 0.50              | 107630.45 | 0.02         | 0.85              |
| 15  | 107745.61 | –0.00        | 0.21              | 107626.60 | 0.04         | 0.63              |
| 16  | 107749.40 | 0.04         | –0.04             | 107622.79 | 0.01         | 0.44              |
| 17  | 107752.95 | –0.10        | –0.53             | 107619.01 | 0.19         | 0.28              |

origin lies near  $107650\text{ cm}^{-1}$ . From the isotope shift of the perturber state (approximately  $60\text{ cm}^{-1}$ ) it seems likely that it is a  $\nu=1$  state. In conclusion we suggest that the  ${}^1\Pi, \nu=2$  state {13} is perturbed and predissociated by an interaction with a state of either  ${}^1\Pi, \nu=1$  or  ${}^1\Delta, \nu=1$  character.

### 3.5. Band systems in the range 93.1–93.3 nm

In the wavelength interval 93.1–93.3 nm Eidelsberg and Rostas [3] identified two band systems, denoted as {15A} and {15B}, that were both tentatively assigned as the  $(5p\pi) {}^1\Pi, \nu=0$  Rydberg state. Furthermore they observed another system, denoted as {15C}, which they assigned as the  $(5p\sigma) {}^1\Sigma^+, \nu=0$  Rydberg state. For {15A} and {15B} a predissociation rate of  $10^{11}\text{ s}^{-1}$  was estimated, and for {15C} a rate of  $10^{10}\text{ s}^{-1}$ . In the present work this interval was reinvestigated. Long sequences of largely broadened structures and additionally, partly superimposed, two transitions to  ${}^1\Sigma^+$  states with narrow resonances, were found.

A spectrum of the system {15C}, recorded from a high-density cold expansion at  $\lambda=93.31\text{ nm}$ , is shown in fig. 6. The band gap indicates that the excited state is indeed a  ${}^1\Sigma^+$  state. Line positions are listed in table 6. A fit to the data resulted in an accurate value for the band origin. An anomalously large  $B$ -constant ( $2.24\text{ cm}^{-1}$ ) is obtained, which is an indication for a perturbation. Although Eidelsberg and Rostas [3] also find a large  $B$ -constant both values do not agree

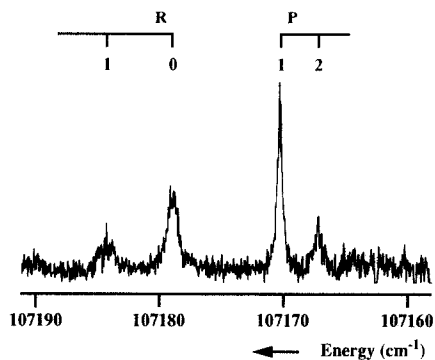


Fig. 6. Recording of a transition to a  ${}^1\Sigma^+$  state {15C} for  ${}^{12}\text{C}^{16}\text{O}$  at  $\lambda=93.30\text{ nm}$ . The rotational dependence of the predissociation rate may be deduced from the anomalously large intensity of P(1). Also note the narrower linewidth of P(1).

Table 6

Observed and calculated line positions (in  $\text{cm}^{-1}$ ) of a  $(5p\sigma) {}^1\Sigma^+, \nu=0-X {}^1\Sigma^+, \nu=0$  transition {15C} of  ${}^{12}\text{C}^{16}\text{O}$  at  $\lambda=93.30\text{ nm}$

| $J$ | $R(J)$    | Obs.–calc. | $P(J)$    | Obs.–calc. |
|-----|-----------|------------|-----------|------------|
| 0   | 107178.94 | 0.04       |           |            |
| 1   | 107184.09 | 0.09       | 107170.59 | 0.01       |
| 2   | 107189.69 | –0.04      | 107167.27 | –0.10      |

within the  $1\sigma$  error margin. The spectrum of fig. 6 is a nice illustration of the consistency between line broadening effects and loss of intensity observed in  $1+1$  photoionization via a predissociated state. The observed linewidth for the P(1) line is  $0.46\pm 0.06\text{ cm}^{-1}$ . For P(2) and R(0) lines, both probing a  $J=1$  level, an averaged value of  $1.1\pm 0.2\text{ cm}^{-1}$  is found. The R(2) line has too low intensity for a reliable determination of its width, but there is an indication that it is even broader. We derive values for predissociation rates  $k_p(J=0)=(3.4\pm 2.0)\times 10^{10}\text{ s}^{-1}$  and  $k_p(J=1)=(1.8\pm 0.5)\times 10^{11}\text{ s}^{-1}$ . So a fourfold increase of the predissociation rate is obtained between  $J=0$  and 1. This is reflected in the line intensities. In a regular spectrum at low temperature the P(1) line is a factor of two weaker than R(0) in a  ${}^1\Sigma^+-{}^1\Sigma^+$  transition (see e.g. figs. 3 and 7). In the present case P(1) is about a factor of two more intense than R(0). So indeed the intensity ratios support in a qualitative sense the conclusion that  $J=1$  predissociates with a rate faster than  $J=0$ .

The wavelength range  $\lambda=93.10\text{--}93.18\text{ nm}$  is shown in fig. 7. Indeed two broadened systems are observed at the positions where Eidelsberg and Rostas [3] located {15A} and {15B}. However in this interval a series of sharp lines appear that are easily identified, particularly in recordings from a cold expansion, as belonging to a  ${}^1\Sigma^+$  state. The line positions are given in table 7. The linewidths are found to correspond to the instrument-limited width and we conclude that the predissociation rate  $k_p$  is below  $3\times 10^{10}\text{ s}^{-1}$ . The intensity pattern of the spectrum recorded from the cold expansion is regular, i.e. is in agreement with a calculated product of Boltzmann and Hönl–London factors. Thus we conclude that no rotationally dependent predissociation effect exists in this newly identified state.

It is not surprising that this band was not uncovered in the photographic absorption study [3]. The

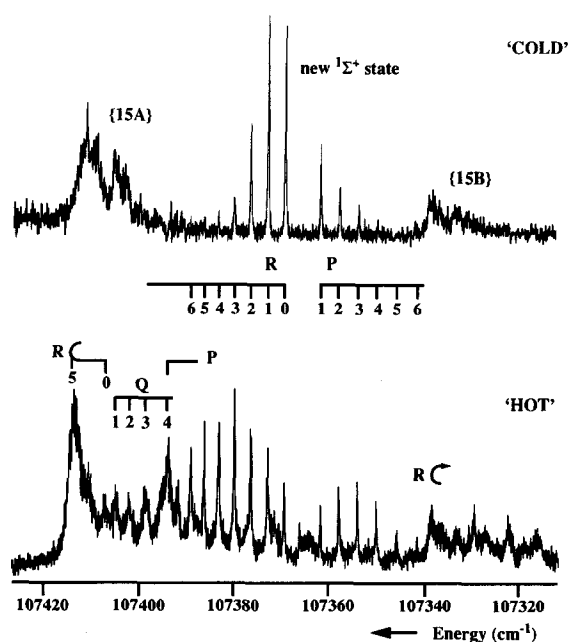


Fig. 7. 1 XUV + 1 UV photoionization spectrum of  $^{12}\text{C}^{16}\text{O}$  in the wavelength interval 93.10–93.18 nm. In between the diffuse bands {15A} and {15B} the newly identified  $(5p\sigma) {}^1\Sigma^+ \nu=0$  state is shown.

Table 7  
Observed and calculated line positions (in  $\text{cm}^{-1}$ ) of the newly assigned  ${}^1\Sigma^+ - X {}^1\Sigma^+$  transition at  $\lambda=93.14$  nm

| $J$ | $R(J)$    | Obs. – calc. | $P(J)$    | Obs. – calc. |
|-----|-----------|--------------|-----------|--------------|
| 0   | 107369.60 | –0.04        |           |              |
| 1   | 107373.27 | –0.05        | 107362.05 | 0.02         |
| 2   | 107376.89 | –0.01        | 107358.11 | 0.01         |
| 3   | 107380.35 | –0.01        | 107354.12 | 0.02         |
| 4   | 107383.71 | 0.04         | 107350.15 | 0.16         |
| 5   | 107386.79 | 0.00         |           |              |
| 6   | 107389.61 | –0.07        |           |              |
| 7   | 107392.41 | 0.13         |           |              |

low intensity in the spectrum combined with the narrow lines indicate that the absorption strength for this transition is weak. Furthermore this band is overlapped by broad features having larger absorption strengths. Our XUV spectrometer, employing 1+1 photoionization, is preferentially sensitive for relatively long-lived excited states.

The  $(5p\sigma) {}^1\Sigma^+ \nu=0$  Rydberg state is expected to lie in the wavelength interval 93.1–93.3 nm. The  $n=3$

and  $n=4$  members of the  $(np\sigma) {}^1\Sigma^+$  series were already identified as the  $\text{C } {}^1\Sigma^+$  and  $\text{K } {}^1\Sigma^+$  states, with quantum defects  $\delta_p=0.7200$  and  $\delta_p=0.6832$  respectively [3]. The  $n=6$  member (state {8B}) has  $\delta_p=0.6660$ . Both {15C} as well as the newly identified state are candidates to be the  $n=5$  term of the  $(np\sigma) {}^1\Sigma^+$  series. Based on this assumption the quantum defects become  $\delta_{\{15C\}}=0.6704$  and  $\delta_\Sigma=0.5978$ . The state {15C} has a  $B$ -constant much larger than that of the  $n=3, 4$  and 6 states. The  $B$ -constant of the newly identified  ${}^1\Sigma^+$  state ( $B=1.884 \text{ cm}^{-1}$ ) agrees much better with the values for  $n=3, 4$  and 6. However, the quantum defects make state {15C} the most likely candidate for the  $(5p\sigma) {}^1\Sigma^+ \nu=0$  Rydberg state. The deviating  $B$ -constant may be attributed to a perturbation. As the newly identified  ${}^1\Sigma^+$  state was observed only for the  $^{12}\text{C}^{16}\text{O}$  isotope a vibrational assignment cannot be given.

The spectrum of the {15A} band, displayed in fig. 7, was not rotationally analyzed. The lines overlap in red-shaded R and Q bandheads and the highest  $J$  members of the P branch, used by Eidelsberg et al. [4] for identification, are rather weak. The bandhead positions of ref. [4] are consistent with present measurements. The identification of the lines of {15A} in fig. 7 is based on the values of Eidelsberg et al. An important conclusion may be drawn on the predissociation rates of the excited state {15A}. From the overlapping features we estimate that the widths of the rotational lines must exceed  $1.5 \text{ cm}^{-1}$ . This results in a predissociation rate of  $k_p > 3 \times 10^{11} \text{ s}^{-1}$ .

Part of the spectrum of the {15B} band is shown at the long wavelength side of fig. 7. The rotational structure appears to be similar to that of the {15A} band and a probable R bandhead is indicated. Such an identification would not be in accordance with the assignment of Eidelsberg et al. [4], who identify the transition as  ${}^1\Pi - X {}^1\Sigma^+$ . They found an R-branch progression towards the blue side of the feature that we now mark as an R bandhead. Although a long progression, with at least fifteen well-resolved rotational lines towards lower energy is observed, it is not possible to consistently identify this series with an unperturbed  ${}^1\Pi - {}^1\Sigma^+$  band. Also the transition frequencies of the lines observed differ markedly from those listed by Eidelsberg et al. [4]. For completeness we list the observed transition frequencies of the {15B} band in table 8. The linewidth of the resolved rota-

Table 8

Observed but unassigned transitions in band {15B} at  $\lambda=93.16$  nm. Values in  $\text{cm}^{-1}$

|                         |           |
|-------------------------|-----------|
| 107337.69 <sup>a)</sup> | 107294.00 |
| 107333.32               | 107290.58 |
| 107329.36               | 107283.15 |
| 107326.97               | 107279.88 |
| 107322.03               | 107275.28 |
| 107316.04               | 107271.51 |
| 107309.03               | 107258.52 |
| 107300.15               | 107245.56 |

<sup>a)</sup> R bandhead.

tional lines is  $1.5 \pm 0.2 \text{ cm}^{-1}$ , resulting in a predissociation rate  $k_p = 2.7 \pm 0.4 \cdot 10^{11} \text{ s}^{-1}$ . No evidence of rotational-state dependent predissociation is found for band {15B}.

At an energy of  $107220.5 \text{ cm}^{-1}$  another, previously unidentified, band feature appeared. The low signal-to-noise and the rather large rotational linewidth, similar to that of {15A} and {15B}, did not allow for a detailed analysis.

### 3.6. The $(3\sigma)W^1\Pi, v=2$ state {18}

Spectra of transitions to the  $(3\sigma)W^1\Pi, v=2$  state {18}, which is the  $n=3$  member of a Rydberg series converging to the  $A^2\Pi$  second ionization limit in  $\text{CO}^+$ , are shown in fig. 8 for the  $^{12}\text{C}^{16}\text{O}$  and  $^{13}\text{C}^{16}\text{O}$  isotopes. At the low energy side of the  $^{12}\text{C}^{16}\text{O}$  spectrum narrow features appear, that can be ascribed to the strong  $b^1\Pi_u-X^1\Sigma_g^+$  (7,0) band of  $\text{N}_2$ , detected from the nitrogen residual background gas in the vacuum chamber. A spectrum for  $^{13}\text{C}^{18}\text{O}$  could not be recorded simultaneously with that of  $^{13}\text{C}^{16}\text{O}$  because of the large isotope shift. Frequency positions of the observed transitions are listed in tables 9 and 10 for  $^{12}\text{C}^{16}\text{O}$  and  $^{13}\text{C}^{16}\text{O}$  respectively. Overlapping Q and P lines were deconvoluted, where the accurate determination of line positions was facilitated by recordings at high and at low molecular beam rotational temperatures. Molecular constants, derived from a minimization routine using eqs. (7) and (8), are listed in table 1. A negative value for the  $A$ -doubling parameter is found, indicating that the  $\Pi_r(J)$  parity levels, probed in the Q branch, are shifted upward with respect to the  $\Pi_e(J)$  states.

Regular red-shaded band patterns, typical for ex-

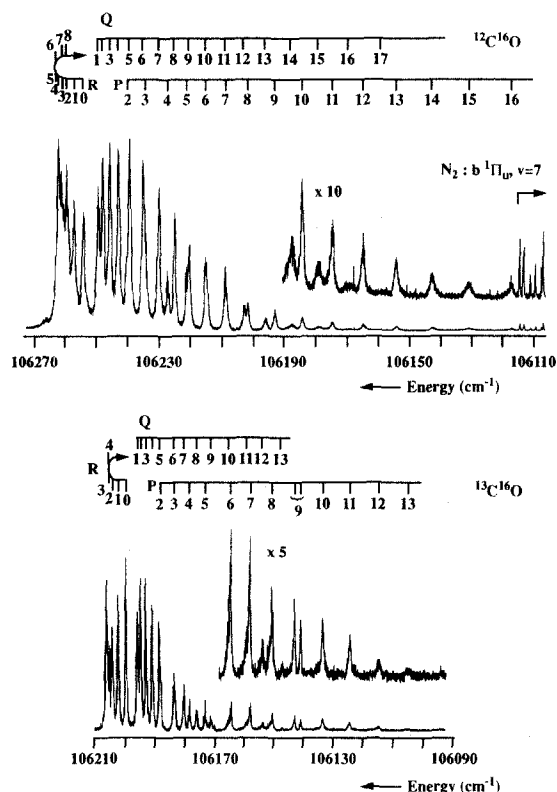


Fig. 8. The transition to the  $W^1\Pi, v=2$  state {18} of  $^{12}\text{C}^{16}\text{O}$  (upper spectrum) and  $^{13}\text{C}^{16}\text{O}$  (lower spectrum). Note the shifted energy scales, corresponding to the isotope shift for a  $v=2$  state. The narrow lines at the long wavelength end are assigned to the  $b^1\Pi_u-X^1\Sigma_g^+$  (7,0) band of  $\text{N}_2$ . Since  $\text{N}_2$  also has mass 28, this contamination is not filtered by the TOF mass selector.

citation of states with a small  $B$ -constant, are observed in the spectra of both  $^{12}\text{C}^{16}\text{O}$  and  $^{13}\text{C}^{16}\text{O}$ . However, closer inspection reveals that several perturbations do occur in the rotational structure. First for both isotopes a negative  $D$ -constant results from the fit. A negative centrifugal distortion effect is a manifestation of a perturbation; however the error margins for the  $D$ -constants are such that unambiguous conclusions may not be drawn. Local perturbations are found as well. For  $^{12}\text{C}^{16}\text{O}$  the  $\Pi_e(J=8)$  state is locally perturbed; the well-resolved P(9) line is red-shifted by  $0.7 \text{ cm}^{-1}$ . This perturbation effect is parity dependent, because no corresponding dislocation of the  $\Pi_r(J=8)$  state is deduced. In the  $^{13}\text{C}^{16}\text{O}$  isotope the  $\Pi_e(J=8)$  state is also found to be locally perturbed. Here two distinct features, one blue-shifted

Table 9

Observed and calculated line positions (in  $\text{cm}^{-1}$ ) of the  $(3s\sigma)W^1\Pi, \nu=2-X^1\Sigma^+, \nu=0$  transition {18} of  $^{12}\text{C}^{16}\text{O}$  at  $\lambda=94.12$  nm. Lines marked with (b) are blended. Lines marked with (w) are weak and not included in the minimization routine. The P(9) line, marked with (\*), was also left out of the fit

| $J$ | $R(J)$       | Obs. – calc. | $Q(J)$       | Obs. – calc. | $P(J)$       | Obs. – calc. |
|-----|--------------|--------------|--------------|--------------|--------------|--------------|
| 0   | 106254.25    | 0.11         |              |              |              |              |
| 1   | 106256.76    | –0.01        | 106250.41    | 0.11         |              |              |
| 2   | 106258.70    | –0.10        | 106249.16    | 0.06         | 106242.74    | 0.14         |
| 3   | 106260.00    | –0.23        | 106247.32    | 0.02         | 106237.53    | –0.02        |
| 4   | 106261.01(b) | –0.04        | 106244.89    | –0.01        | 106231.77    | –0.12        |
| 5   | 106261.01(b) | –0.27        | 106241.92    | 0.01         | 106225.46    | –0.17        |
| 6   | 106260.95(b) | 0.05         | 106238.35    | 0.02         | 106218.24(b) | –0.53        |
| 7   |              |              | 106234.20    | 0.05         | 106211.31(b) | 0.00         |
| 8   |              |              | 106229.52    | 0.13         | 106203.23    | –0.02        |
| 9   |              |              | 106224.43    | 0.39         | 106193.90(*) | –0.70        |
| 10  |              |              | 106218.12(b) | 0.00         | 106185.18    | –0.19        |
| 11  |              |              | 106211.31(b) | –0.31        | 106175.51    | –0.04        |
| 12  |              |              | 106204.49    | –0.06        | 106165.22    | 0.06         |
| 13  |              |              | 106196.92    | 0.01         | 106154.42    | 0.23         |
| 14  |              |              | 106188.65    | –0.07        | 106142.63    | –0.02        |
| 15  |              |              | 106179.88    | –0.09        | 106130.54    | –0.01        |
| 16  |              |              | 106169.68(w) | –1.00        | 106116.74(w) | –1.15        |

Table 10

Observed and calculated line positions (in  $\text{cm}^{-1}$ ) of the  $(3s\sigma)W^1\Pi, \nu=2-X^1\Sigma^+, \nu=0$  transition {18} of  $^{13}\text{C}^{16}\text{O}$  at  $\lambda=94.17$  nm. Lines marked with (b) are blended. Lines marked with (w) are weak and not included in the minimization routine. The P(9) line, marked with (\*), was found as a double line

| $J$ | $R(J)$       | Obs. – calc. | $Q(J)$       | Obs. – calc. | $P(J)$       | Obs. – calc. |
|-----|--------------|--------------|--------------|--------------|--------------|--------------|
| 0   | 106199.46    | –0.04        |              |              |              |              |
| 1   | 106202.04    | 0.07         | 106195.67    | –0.16        |              |              |
| 2   | 106204.07    | 0.22         | 106194.51    | –0.14        | 106188.31    | –0.16        |
| 3   | 106205.79(b) | 0.56         | 106192.80    | –0.09        | 106183.33(b) | –0.27        |
| 4   | 106205.79(b) | –0.18        | 106190.64    | 0.09         | 106178.34    | 0.22         |
| 5   | 106205.79(b) | –0.36        | 106188.07    | 0.41         | 106172.80    | 0.72         |
| 6   |              |              | 106183.33(b) | –0.90        | 106164.58    | –0.88        |
| 7   |              |              | 106180.24    | –0.04        | 106158.23    | –0.06        |
| 8   |              |              | 106175.79    | –0.04        | 106150.88    | 0.28         |
| 9   |              |              | 106170.83    | –0.09        | 106143.26(*) | –1.30        |
| 9   |              |              |              |              | 106141.11(*) | 0.85         |
| 10  |              |              | 106165.41    | –0.16        | 106133.83    | 0.10         |
| 11  |              |              | 106159.55    | –0.27        | 106124.57    | –0.05        |
| 12  |              |              | 106153.94    | 0.23         | 106114.94    | –0.15        |
| 13  |              |              | 106147.33    | 0.05         | 106104.96    | –0.23        |

by  $1.30 \text{ cm}^{-1}$  and one red-shifted by  $0.85 \text{ cm}^{-1}$  were found for the P(9) line. Again this perturbation has no counterpart in the Q branch and is therefore parity dependent. Another local perturbation was found near  $J=5$  in the spectrum for the  $^{13}\text{C}^{16}\text{O}$  isotope; this perturbation is isotope dependent as it does not oc-

cur for  $^{12}\text{C}^{16}\text{O}$ . For the  $\Pi_e$  levels an anti-crossing appears between  $J=4$  and 5; a blue-shift of P(5) and a red-shift of P(6). For the  $\Pi_f$  parity component the anti-crossing is shifted by one  $J$  level. The Q(6) line appeared to be missing, when initially assigning the transitions. However, the P(3) line was found to be

largely broadened and this is attributed to the fact that it is partly overlapped by the shifted Q(6) line. So a perturbation for  $\Pi_r(J)$  is found between  $J=5$  and 6 (see also table 10). Such a parity independent anti-crossing, occurring at different  $J$  for  $\Pi_e$  and  $\Pi_f$  levels may well be explained if the perturber state is a bound state of  $\Pi$  or  $\Delta$  symmetry with a rather large  $A$ -doubling.

The predissociation rates of the  $W^1\Pi, v=2$  state have been reported to be isotope dependent for  $^{12}\text{C}^{16}\text{O}/^{13}\text{C}^{16}\text{O}$  [6]. From the present more accurate data a continuing increase of the predissociation rate at higher  $J$  levels could be deduced. The predissociation effects were found to be parity independent. Line broadening in the Q and P branches follows a similar trend, and therefore widths of  $\Pi_e(J)$  and  $\Pi_f(J)$  components were averaged. Predissociation rates, obtained after deconvolution of the instrumental width from the observed linewidths, are plotted as a function of  $J$  in fig. 9 for both isotopic species. For levels  $J \leq 5$  the rates are found to be rotationally independent, resulting in averaged values  $k_p(^{12}\text{C}^{16}\text{O}) = (1.21 \pm 0.10) \times 10^{11} \text{ s}^{-1}$  and  $k_p(^{13}\text{C}^{16}\text{O}) = (0.75 \pm 0.15) \times 10^{11} \text{ s}^{-1}$ . These predissociation rates for the  $J \leq 5$  levels of the  $W^1\Pi, v=2$  state may be compared with the values for radiative decay  $k_{\text{rad}} = 2.7 \times 10^8 \text{ s}^{-1}$ , obtained in an ab initio calculation [24]. This implies that the predissociation yield

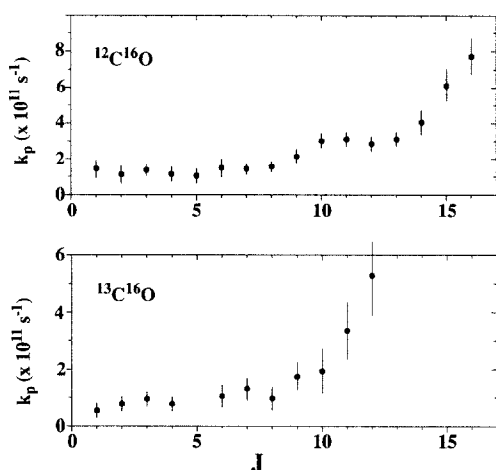


Fig. 9. Rotational-state-dependent predissociation rates for  $W^1\Pi, v=2, J$ -states {18} for  $^{12}\text{C}^{16}\text{O}$  (upper) and  $^{13}\text{C}^{16}\text{O}$  (lower) isotopes. Values were averaged over  $\Pi_e$  and  $\Pi_f$  components.

for this state is 99.8% for  $^{12}\text{C}^{16}\text{O}$  and 99.6% for  $^{13}\text{C}^{16}\text{O}$ . For levels  $J \geq 10$  the predissociation yield is even higher.

### 3.7. The $(4d\sigma)^1\Sigma^+, v=0$ state {19}

A spectrum of the  $(4d\sigma)^1\Sigma^+ - X^1\Sigma^+ (0,0)$  band of  $^{12}\text{C}^{16}\text{O}$  at  $\lambda = 94.63 \text{ nm}$ , recorded under conditions of a near-room-temperature rotational population distribution in the molecular beam, is shown in fig. 10. Several perturbations in the excited state manifest themselves through line broadening, anomalous intensity and frequency shifts. The transition frequencies are listed in table 11. The  $(4d\sigma)^1\Sigma^+ - X^1\Sigma^+ (0,0)$  band is overlapped by a sequence of unassigned lines, marked by (?) in fig. 10. These features,

Table 11  
Observed and calculated line positions (in  $\text{cm}^{-1}$ ) of the  $(4d\sigma)^1\Sigma^+, v=0 - X^1\Sigma^+, v=0$  transition of  $^{12}\text{C}^{16}\text{O}$  at  $\lambda = 94.63 \text{ nm}$

| $J$ | $R(J)$                  | Obs. - calc. | $P(J)$                  | Obs. - calc. |
|-----|-------------------------|--------------|-------------------------|--------------|
| 0   | 105680.13               | 0.04         |                         |              |
| 1   | 105683.80               | -0.02        | 105672.45               | -0.00        |
| 2   | 105687.53               | 0.03         | 105668.61               | 0.06         |
| 3   | 105691.08               | -0.05        | 105664.65               | 0.05         |
| 4   | 105694.58 <sup>a)</sup> | -0.11        | 105660.46               | -0.13        |
| 5   | 105697.81 <sup>a)</sup> | -0.39        | 105656.36               | -0.17        |
| 6   | 105700.77 <sup>a)</sup> | -0.87        | 105652.23 <sup>a)</sup> | -0.17        |
| 7   | 105705.55 <sup>a)</sup> | 0.53         | 105647.91 <sup>a)</sup> | -0.31        |
| 8   | 105708.37               | 0.04         | 105643.31 <sup>a)</sup> | -0.67        |
| 9   | 105711.26 <sup>a)</sup> | -0.32        | 105640.61 <sup>a)</sup> | 0.92         |
| 10  | 105713.87 <sup>a)</sup> | -0.89        | 105635.41               | 0.09         |
| 11  | 105715.87 <sup>a)</sup> | -1.99        | 105630.47 <sup>a)</sup> | -0.42        |
| 12  | 105721.98 <sup>a)</sup> | 1.10         | 105625.54 <sup>a)</sup> | -0.86        |
| 13  | 105724.41 <sup>a)</sup> | 0.58         |                         |              |
| 14  | 105726.94 <sup>a)</sup> | 0.25         | 105618.39               | 1.20         |
| 15  | 105729.54               | 0.09         | 105613.08               | 0.61         |
| 16  | 105732.16               | 0.03         | 105608.00               | 0.33         |
| 17  | 105734.70               | -0.00        | 105602.99               | 0.20         |
| 18  | 105737.30               | 0.12         | 105597.82               | 0.00         |
| 19  | 105739.37               | -0.17        | 105592.72               | -0.03        |
| 20  | 105741.53 <sup>a)</sup> | -0.26        | 105587.65               | 0.06         |
| 21  |                         |              | 105582.18               | -0.14        |
| 22  | 105745.85               | -0.08        | 105576.76 <sup>a)</sup> | -0.18        |
| 23  | 105747.71               | -0.09        |                         |              |
| 24  | 105749.50               | -0.03        | 105565.77               | -0.08        |
| 25  | 105751.19               | 0.07         | 105560.10               | -0.01        |
| 26  | 105752.63               | 0.08         | 105554.23               | -0.02        |
| 27  |                         |              | 105548.30               | 0.06         |

<sup>a)</sup> Lines not included in the minimization routine.

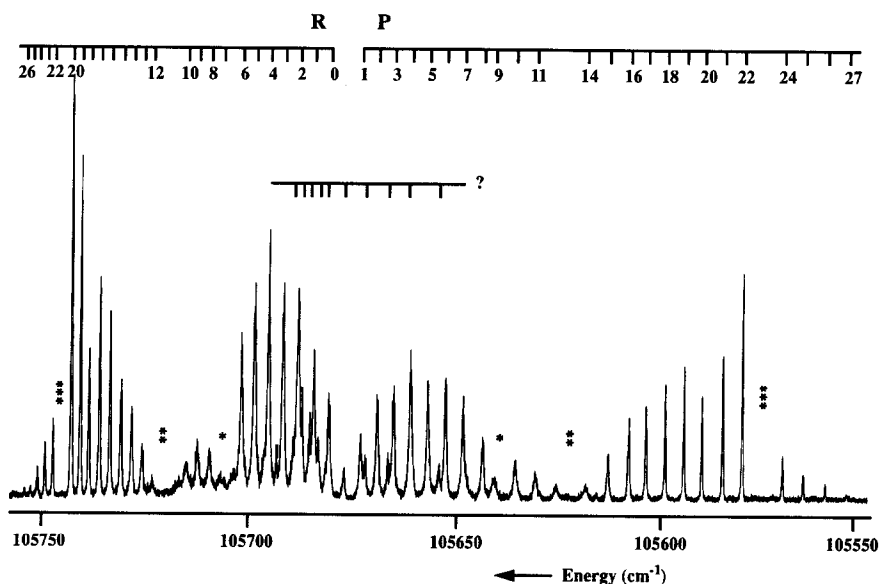


Fig. 10. 1 XUV + 1 UV photoionization spectrum of the  $(4d\sigma) {}^1\Sigma^+ - X {}^1\Sigma^+ (0,0)$  band {19} of  $^{12}\text{C}^{16}\text{O}$  at  $\lambda = 94.63$  nm. Three major perturbations are indicated with (\*), (\*\*) and (\*\*\*). The lines related to the manifold (?) belong to an unidentified band of  $^{12}\text{C}^{16}\text{O}$ .

Table 12

Unidentified transitions in the band at  $\lambda = 94.63$  nm. The low  $J$ -values are obtained from cold expansions, while the high  $J$ -values are obtained from a molecular beam with a higher rotational temperature. Values are in  $\text{cm}^{-1}$

| Low $J$   | High $J$  |
|-----------|-----------|
| 105666.02 | 105653.67 |
| 105668.65 | 105671.38 |
| 105676.25 | 105682.81 |
| 105692.50 | 105686.52 |
| 105695.81 | 105699.13 |

of which the line positions are listed in table 12, belong to another band system of  $^{12}\text{C}^{16}\text{O}$  of which the rotational structure could not be unravelled. Three major local perturbations, associated with drastic intensity variations in the P and R branch of the  $(4d\sigma) {}^1\Sigma^+ - X {}^1\Sigma^+$  band, are indicated in fig. 10. At  $J=8$  and  $J=12$  there is a clear drop of intensity and around these  $J$ -values the lines are broadened. P(23) and R(21) transitions, probing level  $J=22$  in the excited state, are completely missing. This is a clearcut example of an accidental predissociation of the  $J=22$  level. A fourth minor perturbation is found in lines R(18) and P(20) showing a reproducible intensity

drop as well. From the observed linewidths, after deconvolution of the instrumental width, predissociation rates were determined and plotted as a function of  $J$  in the upper part of fig. 11. The combined effect of line broadening and intensity loss is again illus-

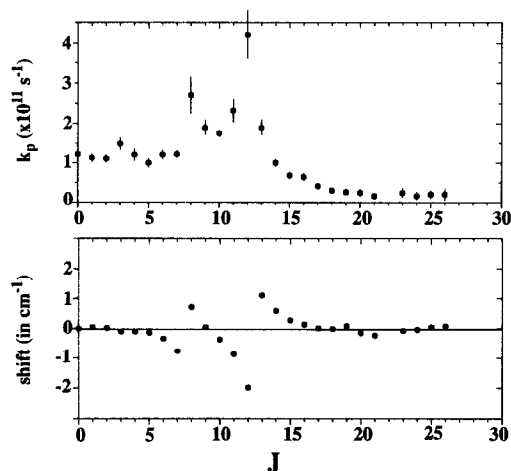


Fig. 11. Upper: Rotational-state-dependent predissociation rates for the  $(4d\sigma) {}^1\Sigma^+, v=0, J$ -states. Lower: shifts, due to perturbations, from diatomic rotor energies (eq. (4)) calculated with the constants listed in table 1.

trated here. The  $J=8$  and 12 levels indeed have the largest predissociation rate. The levels with  $J \leq 5$  have a constant rate of  $(1.2 \pm 0.2) \times 10^{11} \text{ s}^{-1}$ , in agreement with previously reported values [3,7]. At the higher rotational states up to  $J=21$  line narrowing, accompanied by intensity increase is observed.

The intensities of transitions to the  $J=19$  level deviate by about 20% from the regular but anomalous pattern of increasing intensity towards higher  $J$ -states. Following the reasoning of the appendix on the dependence of intensity on the excited state lifetime, this is evidence of an extra accidental coupling, although weak, to a bound perturber state.

The same perturbations that affect intensities and linewidths, also cause shifts in line positions. The observed transition frequencies were first fitted to the expression for a simple rotor (eq. (6)). Next the lines that are found to be perturbed were left out of the final fit. The deviations between observed and calculated rotational energies are plotted as a function of  $J$  in the lower part of fig. 11. A comparison of the two parts of this figure reveals that indeed the rotational levels that are broadened are also shifted. Levels  $J=8$  and 12 are located at consecutive anti-crossings. We find that the three major perturbation effects have sharply defined rotational dependencies and must therefore be related to couplings with bound perturber states.

### 3.8. The $(4p\pi)L^1\Pi, v=0$ state {25}

The  $(4p\pi)L^1\Pi-X^1\Sigma^+(0,0)$  band {25} was found to be the most intense feature in CO in the wavelength range 91–98 nm, when using 1+1 photoionization. A spectrum of this band at  $\lambda=96.83$  nm is shown for  $^{12}\text{C}^{16}\text{O}$  in fig. 12. The rotational structure is found to be completely regular, with one exception. The molecular constants obtained from a fit to eqs. (7) and (8) are given in table 1. Observed transition frequencies are listed in table 13. The Q(7) line is missing. This was observed before by opticalgalvanic spectroscopy [25] and attributed to an accidental predissociation of the  $\Pi_f(7)$  state. The linewidths in the Q branch were found to be instrument limited at  $0.30 \text{ cm}^{-1}$ . Even up to the highest  $J$ -values no additional broadening effects were observed. We therefore estimate a predissociation rate  $k_p < 3 \times 10^{10} \text{ s}^{-1}$  for the  $\Pi_f(J)$  parity components. This observation is in agreement with data of Drabbels et al. [8], who determined  $k_p = 1.9 \times 10^9 \text{ s}^{-1}$ . A corresponding value for the lifetime of 0.55 ns is certainly consistent with the high signal yield observed in the present study.

In the P and R branches a gradual line broadening effect towards higher  $J$ -values was observed. In fig. 13 derived predissociation rates are plotted. The accurate values for predissociation rates of  $\Pi_e(J \leq 4)$

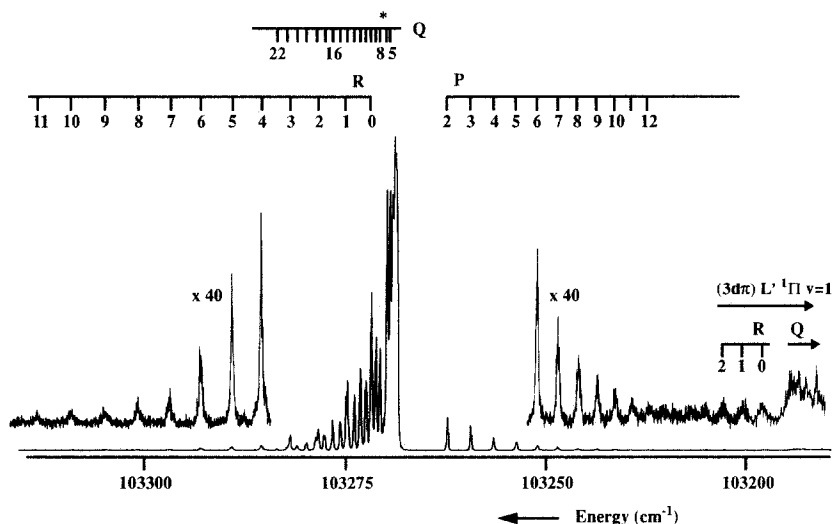


Fig. 12. Spectrum of transition to the  $(4p\pi)L^1\Pi, v=0$  state {25} and part of the  $(3d\pi)L^1\Pi, v=1$  state {26} for  $^{12}\text{C}^{16}\text{O}$ . Note the increasing linewidth in the R and P branch of the L–X band. The Q(7) line, marked with (\*) is missing due to an accidental predissociation.

Table 13

Observed and calculated line positions (in  $\text{cm}^{-1}$ ) of the  $4p\pi L^1\Pi$ ,  $v=0-X^1\Sigma^+$ ,  $v=0$  transition {25} of  $^{12}\text{C}^{16}\text{O}$  at  $\lambda=96.83$  nm

| $J$ | $R(J)$    | Obs. – calc. | $Q(J)$    | Obs. – calc. | $P(J)$    | Obs. – calc. |
|-----|-----------|--------------|-----------|--------------|-----------|--------------|
| 0   | 103275.66 | –0.14        |           |              |           |              |
| 1   | 103279.80 | –0.09        | 103271.80 | –0.12        |           |              |
| 2   | 103283.94 | –0.14        |           |              | 103264.25 | –0.02        |
| 3   | 103288.30 | –0.10        |           |              | 103260.65 | –0.01        |
| 4   | 103292.92 | 0.09         | 103272.73 | 0.14         | 103257.16 | –0.01        |
| 5   | 103297.39 | 0.02         | 103273.08 | 0.11         | 103253.71 | –0.08        |
| 6   | 103302.06 | 0.02         | 103273.53 | 0.11         | 103250.60 | 0.06         |
| 7   | 103306.78 | –0.03        | missing   |              | 103247.50 | 0.10         |
| 8   | 103311.72 | 0.01         | 103274.61 | 0.07         | 103244.40 | 0.02         |
| 9   | 103316.67 | –0.05        | 103275.27 | 0.06         | 103241.52 | 0.04         |
| 10  | 103321.75 | –0.09        | 103275.95 | –0.00        | 103238.68 | –0.02        |
| 11  | 103326.89 | –0.20        | 103276.78 | 0.01         | 103236.11 | 0.08         |
| 12  |           |              | 103277.64 | –0.02        | 103233.55 | 0.06         |
| 13  |           |              | 103278.57 | –0.07        |           |              |
| 14  |           |              | 103279.57 | –0.11        |           |              |
| 15  |           |              | 103280.77 | –0.03        |           |              |
| 16  |           |              | 103281.96 | –0.03        |           |              |
| 17  |           |              | 103283.27 | 0.01         |           |              |
| 18  |           |              | 103284.62 | 0.02         |           |              |
| 19  |           |              | 103286.03 | 0.03         |           |              |
| 20  |           |              | 103287.50 | 0.01         |           |              |
| 22  |           |              | 103290.66 | 0.00         |           |              |

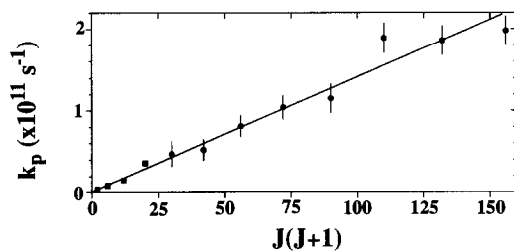


Fig. 13. Rotational-state-dependent predissociation rates for the  $\Pi_e$  components of the  $(4p\pi)L^1\Pi$ ,  $v=0$  state as a function of  $J(J+1)$ . Data points for  $J \leq 4$  (■) were taken from ref. [8]. For the  $\Pi_f$  component a predissociation rate  $k_p < 3 \times 10^{10} \text{ s}^{-1}$  was found.

states, determined by Drabbels et al. [8], are included as well. These values agree, within error limits, with the present less accurate values. Drabbels et al. interpret the predissociation mechanism for the L state as originating from a heterogeneous perturbation with a state of  $^1\Sigma^+$  symmetry. In such a case the  $\Pi_f$  parity components are not affected as is indeed observed. Moreover the perturbation with  $\Pi_e$  components is governed by matrix elements

$\langle \Pi_e | H_{\text{int}} | ^1\Sigma^+ \rangle$ , which show a  $\sqrt{J(J+1)}$  dependence [22]. If no particular rotationally dependent resonances occur, e.g. in the case of a repulsive  $^1\Sigma^+$  potential, the predissociation rate is expected to be of the form

$$k_p(J) = k_0 + k_J J(J+1). \quad (14)$$

A plot of the total set of data for the predissociation rate as a function of  $J(J+1)$  (see fig. 13) shows indeed good agreement with the functional form of eq. (14). The intercept at the ordinate is determined by the accurate values at low  $J$ , resulting in  $k_0 = (1.9 \pm 0.2) \times 10^9 \text{ s}^{-1}$ , whereas the slope yields  $k_J = (1.37 \pm 0.05) \times 10^9 \text{ s}^{-1}$ . The present analysis thus strongly indicates that the L  $^1\Pi$  state predissociates by an interaction with a repulsive state.

For  $^{13}\text{C}^{16}\text{O}$  and  $^{13}\text{C}^{18}\text{O}$  spectra of the L–X (0,0) band were recorded as well. They are shown in fig. 14. In both bands no significant predissociation effects could be inferred from the linewidths. Only for the  $\Pi_e$  ( $J \geq 13$ ) states of  $^{13}\text{C}^{16}\text{O}$  line broadening seems to occur, but in view of the limited signal-to-noise in these transitions this is not further analyzed. The ro-

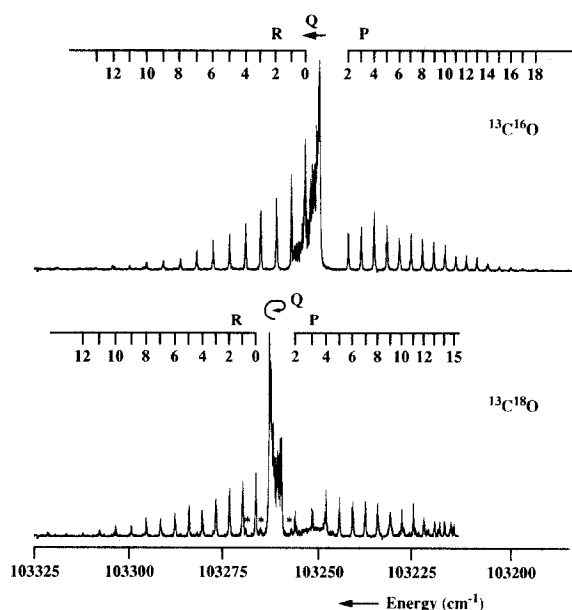


Fig. 14. Spectra of the  $(4\pi)L^1\Pi-X^1\Sigma^+(0,0)$  bands {25} for  $^{13}\text{C}^{16}\text{O}$  (upper) and  $^{13}\text{C}^{18}\text{O}$  (lower). Lines marked with (\*) in the  $^{13}\text{C}^{18}\text{O}$  spectrum are blends from  $^{13}\text{C}^{16}\text{O}$ . The broad feature underneath the P(3) and P(4) lines in the  $^{13}\text{C}^{18}\text{O}$  spectrum corresponds to the Q branch of  $^{13}\text{C}^{16}\text{O}$ . The lines in between high  $J$  members of the P branch can be assigned as R lines of the newly observed  $^1\Pi$  state of  $^{13}\text{C}^{18}\text{O}$  (see also fig. 15). Note the doubly shaded Q branch of  $^{13}\text{C}^{18}\text{O}$  (see text).

tational structure of the L–X (0,0) band of  $^{13}\text{C}^{16}\text{O}$  is found to be regular. The observed line positions are given in table 14 and the molecular constants are included in table 1. The Q branch could not be resolved; so the  $B$ -constant also includes a contribution of the  $A$ -doubling parameter, which could not be determined.

The observed line positions of the L–X (0,0) band of  $^{13}\text{C}^{18}\text{O}$  are listed in table 15. The rotational structure is found to be regular up to  $J=8$ , but for levels  $J \geq 9$  increasing blue-shifts of the rotational levels are deduced (see table 15). The odd pattern of the unresolved, doubly shaded Q branch can also be explained from a blue-shift of the high  $J\Pi_r$  components. This will give rise to a second blue-shaded Q bandhead. So similar to the perturbation in the  $\Pi_c$  levels at high  $J$ -values the  $\Pi_r$  levels are also shifted upward in energy for high  $J$ . This shows that the perturbation found in the rotational structure of the  $(4\pi)L^1\Pi$  state is parity independent.

Table 14

Observed and calculated line positions (in  $\text{cm}^{-1}$ ) of the  $4\pi L^1\Pi$ ,  $\nu=0-X^1\Sigma^+$ ,  $\nu=0$  transition {25} for  $^{13}\text{C}^{16}\text{O}$  at  $\lambda=96.85$  nm

| $J$ | $R(J)$    | Obs. – calc. | $P(J)$    | Obs. – calc. |
|-----|-----------|--------------|-----------|--------------|
| 0   | 103252.75 | 0.11         |           |              |
| 1   | 103256.58 | 0.05         |           |              |
| 2   | 103260.50 | –0.02        | 103241.71 | 0.10         |
| 3   | 103264.64 | 0.03         | 103238.23 | 0.08         |
| 4   | 103268.66 | –0.13        | 103234.82 | 0.03         |
| 5   | 103272.93 | –0.12        | 103231.45 | –0.08        |
| 6   | 103277.39 | 0.01         | 103228.27 | –0.09        |
| 7   | 103281.77 | –0.00        | 103225.23 | –0.05        |
| 8   | 103286.15 | –0.06        | 103222.28 | 0.01         |
| 9   | 103290.66 | –0.01        | 103219.32 | 0.01         |
| 10  | 103295.08 | –0.06        | 103216.35 | –0.05        |
| 11  | 103299.55 | –0.06        | 103213.51 | –0.02        |
| 12  | 103303.94 | –0.10        | 103210.72 | 0.06         |
| 13  | 103308.57 | 0.15         | 103207.91 | 0.11         |
| 14  |           |              | 103205.06 | 0.16         |
| 15  |           |              | 103202.01 | 0.06         |
| 16  |           |              | 103198.90 | –0.03        |
| 17  |           |              | 103195.81 | –0.00        |
| 18  |           |              | 103192.20 | –0.36        |

Table 15

Observed and calculated line positions (in  $\text{cm}^{-1}$ ) of the  $4\pi L^1\Pi$ ,  $\nu=0-X^1\Sigma^+$ ,  $\nu=0$  transition {25} for  $^{13}\text{C}^{18}\text{O}$  at  $\lambda=96.84$  nm

| $J$ | $R(J)$                  | Obs. – calc. | $P(J)$                  | Obs. – calc. |
|-----|-------------------------|--------------|-------------------------|--------------|
| 0   | 103265.96               | –0.01        |                         |              |
| 1   | 103269.45               | –0.06        |                         |              |
| 2   | 103272.98               | –0.09        | 103255.58               | 0.09         |
| 3   | 103276.60               | –0.06        | 103252.11               | 0.07         |
| 4   | 103280.32               | 0.05         | 103248.76               | 0.14         |
| 5   | 103283.87               | –0.03        | 103245.21               | –0.02        |
| 6   | 103287.59               | 0.03         | 103241.80               | –0.06        |
| 7   | 103291.35               | 0.12         | 103238.41               | –0.10        |
| 8   | 103295.12 <sup>a)</sup> | 0.20         | 103235.11               | –0.07        |
| 9   | 103299.10 <sup>a)</sup> | 0.47         | 103231.86               | –0.02        |
| 10  | 103303.31 <sup>a)</sup> | 0.95         | 103228.80 <sup>a)</sup> | 0.21         |
| 11  | 103307.54 <sup>a)</sup> | 1.44         | 103225.82 <sup>a)</sup> | 0.49         |
| 12  | 103311.83 <sup>a)</sup> | 1.98         | 103223.08 <sup>a)</sup> | 1.00         |
| 13  | 103316.22 <sup>a)</sup> | 2.60         | 103220.32 <sup>a)</sup> | 1.46         |
| 14  | 103321.03 <sup>a)</sup> | 3.64         | 103217.65 <sup>a)</sup> | 2.01         |
| 15  |                         |              | 103215.22 <sup>a)</sup> | 2.77         |
| 16  |                         |              | 103212.89 <sup>a)</sup> | 3.62         |
| 17  |                         |              | 103210.74 <sup>a)</sup> | 4.64         |

<sup>a)</sup> Lines not included in the minimization routine.

The band origins of the L–X (0,0) transition are found at 103248.85 and 103262.45  $\text{cm}^{-1}$  for  $^{13}\text{C}^{16}\text{O}$  and  $^{13}\text{C}^{18}\text{O}$  respectively. Eidelsberg et al. reported,

after recalibration of their data [26], reverse values of 103260.9 and 103250.3  $\text{cm}^{-1}$  respectively. In the present XUV-laser setup mass selected spectra are recorded after 1+1 photoionization, whereas Eidelsberg et al. measured absorption in a mixture of  $^{13}\text{C}^{16}\text{O}$  and  $^{13}\text{C}^{18}\text{O}$  [3]. The present identification therefore seems more appropriate.

### 3.9. The $(3d\pi)L' \ ^1\Pi, v=1$ state {26}

Rather weak spectra of transitions to the  $(3d\pi)L' \ ^1\Pi, v=1$  state {26} were obtained for  $^{12}\text{C}^{16}\text{O}$  and  $^{13}\text{C}^{16}\text{O}$  at respectively  $\lambda=96.89$  nm and  $\lambda=96.94$  nm. In fig. 12 the R branch of the  $L'-X$  (1,0) band is shown, adjacent to the P branch of the  $L-X$  (0,0) band of  $^{12}\text{C}^{16}\text{O}$ . The spectra are weak because of a fast predissociation, also visible as strong line broadening of the rotational lines. For both isotopomers we estimate  $k_p=(2.7\pm 0.9)\times 10^{11}$   $\text{s}^{-1}$ , which is in case of  $^{12}\text{C}^{16}\text{O}$  in agreement with the more accurate value of Drabbel et al. [8]. They also reported that the predissociation effect is parity and rotational state independent. Although the present data have a poor signal-to-noise ratio, the state independence of the predissociation rate, also for  $^{13}\text{C}^{16}\text{O}$ , is confirmed. No improvement in accuracy for the molecular constants of the  $L'$  state of  $^{12}\text{C}^{16}\text{O}$  is found over existing values obtained by optogalvanic spectroscopy [27]. For  $^{13}\text{C}^{16}\text{O}$  the data of Eidelsberg and Rostas [3] are not unambiguous. Transition frequencies for  $^{13}\text{C}^{16}\text{O}$  are given in table 16. The R branch is separated from the overlapping Q and P branch. The Q-branch lines are not resolved and only some higher- $J$  members of the P branch could be identified. Derived molecular constants are listed in table 1.

Table 16  
Observed and calculated line positions (in  $\text{cm}^{-1}$ ) of the  $3d\pi L' \ ^1\Pi, v=0-X \ ^1\Sigma^+, v=0$  transition {26} for  $^{13}\text{C}^{16}\text{O}$  at  $\lambda=96.94$  nm

| $J$ | $R(J)$    | Obs. – calc. | $P(J)$    | Obs. – calc. |
|-----|-----------|--------------|-----------|--------------|
| 0   | 103164.88 | 0.16         |           |              |
| 1   | 103167.92 | 0.11         |           |              |
| 5   |           |              | 103139.69 | –0.30        |
| 6   |           |              | 103134.75 | –0.08        |
| 7   |           |              | 103129.29 | –0.08        |
| 8   |           |              | 103123.81 | 0.20         |

### 3.10. A newly observed $^1\Pi$ state for $^{13}\text{C}^{18}\text{O}$

At a band origin of 103203.07  $\text{cm}^{-1}$  ( $\lambda=96.90$  nm) a regular band spectrum of a  $^1\Pi-^1\Sigma^+$  transition, consisting of narrow lines, was observed for  $^{13}\text{C}^{18}\text{O}$  (see fig. 15). The transition frequencies are listed in table 17 and the results of a fit, using eqs. (7) and (8) are included in table 1. The linewidths are found to be instrument limited, resulting in a predissociation rate  $k_p < 3 \times 10^{10}$   $\text{s}^{-1}$ . No local perturbations in the form of shifts, line broadenings or anomalous intensities are found in this band. However, a large  $A$ -doubling is found, with a negative sign, indicating that the  $\Pi_e$  components are shifted downward in energy with respect to  $\Pi_f$ . The value of the  $A$ -doubling parameter fully depends on the correct assignment of Q-lines, that were resolved only for  $J \geq 7$ . An assignment with  $J$  shifted by one unit is also possible, resulting in a different value of  $q$ . However, the identification (in table 17) assuming an unperturbed rotational structure of  $\Pi_f$  levels, yields by far the best convergence in a minimization routine.

The question arises whether the excited  $^1\Pi$  state can be identified as the  $(3d\pi)L' \ ^1\Pi, v=1$  state of  $^{13}\text{C}^{18}\text{O}$ . A major difference with the two other isotopes is that the rate of predissociation is an order of magnitude lower. A comparison of molecular constants does not

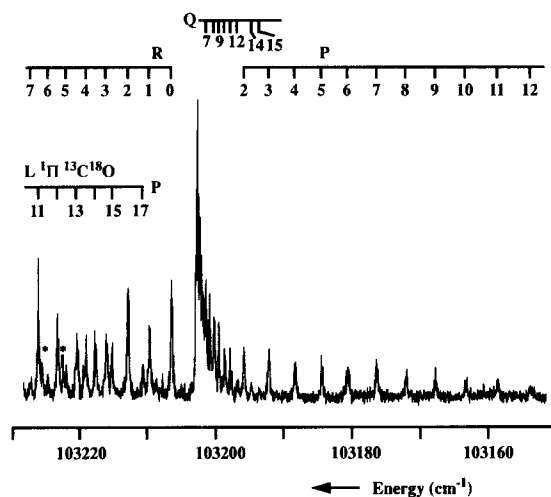


Fig. 15. Spectrum of a transition to a newly observed  $^1\Pi$  state in  $^{13}\text{C}^{18}\text{O}$ . High  $J$  members of the P branch of the  $L-X$  (0,0) band of  $^{13}\text{C}^{18}\text{O}$  are shown as well. Several spectral lines, indicated by (\*), correspond to  $^{13}\text{C}^{16}\text{O}$  lines of the  $L-X$  (0,0) band.

Table 17

Observed and calculated line positions (in  $\text{cm}^{-1}$ ) of a newly observed  ${}^1\Pi\text{-X } {}^1\Sigma^+$ ,  $\nu=0$  transition for  ${}^{13}\text{C}^{18}\text{O}$  at  $\lambda=96.89$  nm

| $J$ | $R(J)$    | Obs. – calc. | $Q(J)$    | Obs. – calc. | $P(J)$    | Obs. – calc. |
|-----|-----------|--------------|-----------|--------------|-----------|--------------|
| 0   | 103206.51 | 0.06         |           |              |           |              |
| 1   | 103209.76 | 0.03         |           |              |           |              |
| 2   | 103212.89 | –0.01        |           |              | 103195.95 | –0.02        |
| 3   | 103216.04 | 0.07         |           |              | 103192.29 | 0.02         |
| 4   | 103219.06 | 0.14         |           |              | 103188.43 | –0.03        |
| 5   |           |              |           |              | 103184.51 | –0.03        |
| 6   | 103224.51 | 0.00         |           |              | 103180.49 | –0.02        |
| 7   | 103227.05 | –0.08        | 103200.90 | –0.01        | 103176.34 | –0.04        |
| 8   |           |              | 103200.30 | 0.01         | 103172.09 | –0.04        |
| 9   |           |              | 103199.62 | 0.03         | 103167.83 | 0.05         |
| 10  |           |              | 103198.78 | –0.02        | 103163.33 | 0.01         |
| 11  |           |              | 103197.92 | –0.02        | 103158.89 | 0.14         |
| 12  |           |              | 103196.87 | –0.11        |           |              |
| 13  |           |              | 103195.95 | –0.02        |           |              |
| 14  |           |              | 103194.83 | –0.01        |           |              |
| 15  |           |              | 103193.68 | 0.07         |           |              |

give an unambiguous answer. The  $B$ -constant for  ${}^{13}\text{C}^{18}\text{O}$ , determined at  $1.708\text{ cm}^{-1}$ , is expected to be smaller than that for  ${}^{13}\text{C}^{16}\text{O}$ , presently determined at  $1.69\text{ cm}^{-1}$ . This is obviously not the case. However, the  $B$  constant of  $1.8773\text{ cm}^{-1}$  for  ${}^{12}\text{C}^{18}\text{O}$  [3] also is anomalously large, so a consistent conclusion cannot be drawn. For  ${}^{12}\text{C}^{18}\text{O}$  a band origin of  $103152.3\text{ cm}^{-1}$  was reported [3], clearly red-shifted from the band origin of  ${}^{12}\text{C}^{16}\text{O}$ . These authors concluded that the  $L'$  state observed must have  $\nu=1$ . For a  $\nu=1$  state the band origin of  ${}^{13}\text{C}^{18}\text{O}$  would have to be further red-shifted, in disagreement with the present observation ( $\nu_0=103203.07\text{ cm}^{-1}$ ). Thus the identification of the newly observed  ${}^1\Pi$  state for  ${}^{13}\text{C}^{18}\text{O}$  is left as an open question.

### 3.11. The $(4p\sigma)K^1\Sigma^+$ , $\nu=0$ state {27}

Strong  $1+1$  photoionization spectra of the  $(4p\sigma)K^1\Sigma^+ - X^1\Sigma^+$  (0,0) bands {27} of  ${}^{12}\text{C}^{16}\text{O}$ ,  ${}^{13}\text{C}^{16}\text{O}$  and  ${}^{13}\text{C}^{18}\text{O}$  were obtained near  $\lambda=97.03\text{ nm}$  (see fig. 16). For  ${}^{12}\text{C}^{16}\text{O}$  the spectrum of this completely regular band was analyzed previously [6]. Drabbels et al. [8] determined an accurate value for the predissociation rate for the rotational states  $J \leq 4$ :  $k_p = (2.22 \pm 0.13) \times 10^{10}\text{ s}^{-1}$ . Moreover  $k_p$  was found to be independent of  $J$  for these low  $J$ -values. From the regular intensity distribution in fig. 16 it may be

concluded that the predissociation rate is constant up to  $J=20$ .

The transition frequencies in the  $K\text{-X}$  band of  ${}^{13}\text{C}^{16}\text{O}$  are listed in table 18. All data points fit properly to a simple rotor expression (eq. (6)). The resulting molecular constants are included in table 1. Line broadening effects are hardly discernable, so  $k_p$  is estimated to be  $\leq 3 \times 10^{10}\text{ s}^{-1}$ .

The spectrum of the  $K\text{-X}$  band of  ${}^{13}\text{C}^{18}\text{O}$  is perturbed. Large frequency shifts, observed in  $P$  and  $R$  branches near  $J=8\text{-}9$ , are accompanied by strong intensity changes. This indicates that the  $(4p\sigma)K^1\Sigma^+$ ,  $\nu=0$  state is locally perturbed by a bound state, which is, in turn, strongly predissociated. The nature of this perturbation was examined in detail in a separate study [23], where the transition frequencies are listed. There it was shown that the perturbation has a heterogeneous character and it was suggested that the perturber is the  $E^1\Pi$ ,  $\nu=5$  state. From a deperturbation analysis accurate molecular constants of the perturber state, included in table 1, could be derived as well.

### 3.12. The $(3s\sigma)W^1\Pi$ , $\nu=0$ state {28}

Transitions to the  $(3s\sigma)W^1\Pi$ ,  $\nu=0$  state {28} were

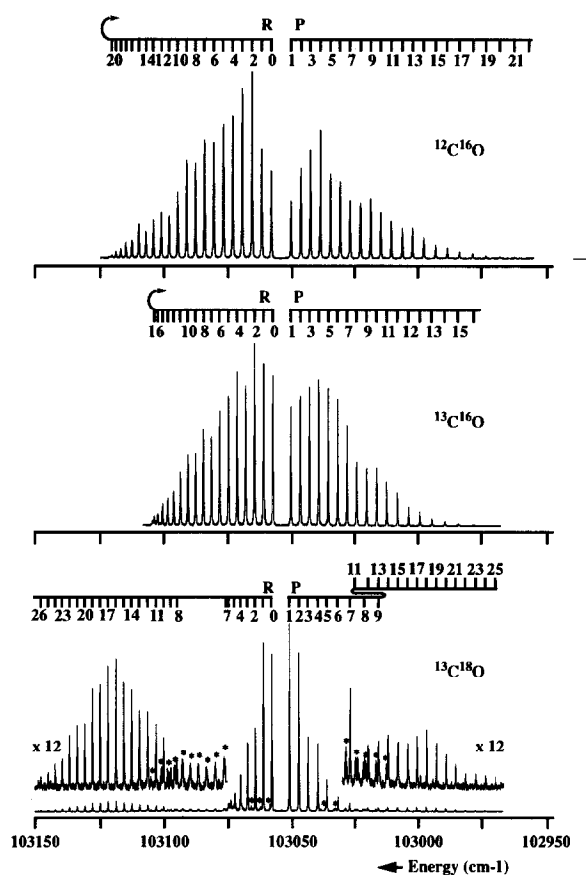


Fig. 16. The  $(4p\sigma)K'\Sigma^+-X'\Sigma^+(0,0)$  bands {27} of  $^{12}\text{C}^{16}\text{O}$ ,  $^{13}\text{C}^{16}\text{O}$  and  $^{13}\text{C}^{18}\text{O}$ . The lower spectrum is contaminated by lines originating from  $^{13}\text{C}^{16}\text{O}$ , indicated by (\*). Note the strong perturbation at  $J=8-9$  in the excited state of  $^{13}\text{C}^{18}\text{O}$ , manifesting itself via intensity variations and level shifts.

found to be strong and spectra were obtained for the three isotopes. Recordings taken from nearly room temperature molecular beams are shown in fig. 17. The heavier isotopes have slightly red-shifted band origins, typical for a  $\nu=0$  state. Line positions for the rotationally resolved transitions are listed in tables 19–21 for  $^{12}\text{C}^{16}\text{O}$ ,  $^{13}\text{C}^{16}\text{O}$  and  $^{13}\text{C}^{18}\text{O}$  respectively. In minimization routines, using eqs. (7) and (8) good convergence was found for the bands of  $^{13}\text{C}^{16}\text{O}$  and  $^{13}\text{C}^{18}\text{O}$ . Here a negative value for the  $A$ -doubling parameter  $q$  indicates a downward shift of  $\Pi_e(J)$  levels. For  $^{12}\text{C}^{16}\text{O}$  the Q branch was found to be perturbed at the high  $J$ -values ( $J \geq 17$ ). Omitting these lines a consistent fit was obtained with a standard deviation

Table 18

Observed and calculated line positions (in  $\text{cm}^{-1}$ ) of the  $K'\Sigma^+-X'\Sigma^+$ ,  $\nu=0-X'\Sigma^+$ ,  $\nu=0$  transition {27} of  $^{13}\text{C}^{16}\text{O}$  at  $\lambda=97.03$  nm

| $J$ | $R(J)$    | Obs. – calc. | $P(J)$    | Obs. – calc. |
|-----|-----------|--------------|-----------|--------------|
| 0   | 103058.10 | 0.03         |           |              |
| 1   | 103061.75 | 0.03         | 103050.86 | 0.12         |
| 2   | 103065.36 | 0.02         | 103047.13 | 0.08         |
| 3   | 103068.96 | 0.03         | 103043.40 | 0.06         |
| 4   | 103072.36 | –0.13        | 103039.65 | 0.04         |
| 5   | 103075.86 | –0.14        | 103036.01 | 0.16         |
| 6   | 103079.34 | –0.10        | 103032.02 | –0.04        |
| 7   | 103082.72 | –0.08        | 103028.18 | –0.04        |
| 8   | 103086.02 | –0.04        | 103024.22 | –0.10        |
| 9   | 103089.21 | 0.01         | 103020.19 | –0.15        |
| 10  | 103092.19 | –0.02        | 103016.14 | –0.12        |
| 11  | 103095.07 | 0.03         | 103012.07 | 0.01         |
| 12  | 103097.69 | 0.02         | 103007.74 | 0.01         |
| 13  | 103100.12 | 0.03         | 103003.22 | –0.01        |
| 14  | 103102.26 | 0.02         | 102998.64 | 0.11         |
| 15  | 103104.19 | 0.09         | 102993.77 | 0.15         |
| 16  | 103105.54 | –0.09        | 102988.59 | 0.14         |
| 17  |           |              | 102983.04 | 0.05         |
| 18  |           |              | 102976.98 | –0.23        |

of  $0.05 \text{ cm}^{-1}$ . Resulting molecular parameters are listed in table 1.

A rotational-state and parity dependent predissociation effect is evident in the spectra of  $^{12}\text{C}^{16}\text{O}$  and  $^{13}\text{C}^{16}\text{O}$ . In the insets in fig. 17 it is shown that the higher members of the P branch exhibit distinct line broadening accompanied by a sharp drop in intensity, whereas the Q-branch lines remain narrow and follow a regular intensity pattern. For the  $^{13}\text{C}^{18}\text{O}$  isotope such a line broadening effect is not observed; there also the P-branch lines remain narrow. Drabbels et al. [8] measured linewidths for  $J \leq 4$  states (of  $^{12}\text{C}^{16}\text{O}$ ) and also found parity and rotational-state dependent predissociation. For the  $\Pi_f$  levels they determined  $k_p = (9.6 \pm 0.8) \times 10^9 \text{ s}^{-1}$ . From the regular intensity pattern it may be concluded that the predissociation rate is constant up to the highest  $J$ -values.

For the  $\Pi_e$  levels the analysis of Drabbels et al. was extended in the present work to include higher  $J$ -values and to  $^{13}\text{C}^{16}\text{O}$ . Predissociation rates for  $\Pi_e(J)$  were derived from line broadening in the P branch and the results are plotted in fig. 18 for  $^{12}\text{C}^{16}\text{O}$  as well as  $^{13}\text{C}^{16}\text{O}$ . Similar to the  $L^1\Pi$  state a linear proportionality with  $J(J+1)$  is found for the predissociation rates. We conclude that the mechanism causing

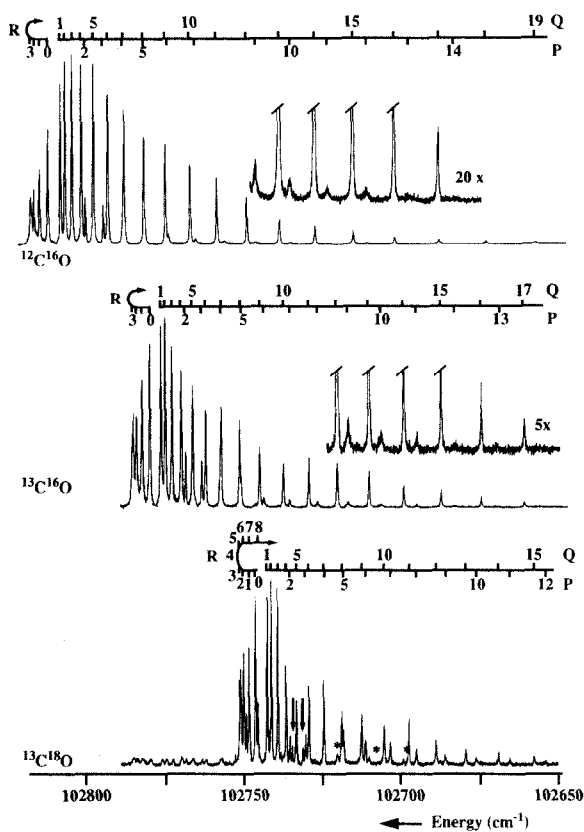


Fig. 17. The  $(3\sigma)W^1\Pi-X^1\Sigma^+(0,0)$  bands {28} of  $^{12}\text{C}^{16}\text{O}$ ,  $^{13}\text{C}^{16}\text{O}$  and  $^{13}\text{C}^{18}\text{O}$ . Note the line broadening in the high  $J$  members of the P branch for  $^{12}\text{C}^{16}\text{O}$  and  $^{13}\text{C}^{16}\text{O}$ . The lower spectrum is contaminated by lines originating from  $^{13}\text{C}^{16}\text{O}$ , indicated by (\*).

the predissociation of the  $W^1\Pi$ ,  $v=0$  state may well be an interaction with a purely dissociative  $^1\Sigma^+$  state. The proportionality constant  $k_J$  (see eq. (14)) is smaller for the heavier  $^{13}\text{C}^{16}\text{O}$  isotope than for  $^{12}\text{C}^{16}\text{O}$ :  $k_J = (1.3 \pm 0.2) \times 10^9 \text{ s}^{-1}$  for  $^{13}\text{C}^{16}\text{O}$  and  $k_J = (2.2 \pm 0.2) \times 10^9 \text{ s}^{-1}$  for  $^{12}\text{C}^{16}\text{O}$ . Although no specific value may be derived it may nevertheless be stated that the constant  $k_J$  for  $^{13}\text{C}^{18}\text{O}$  is smaller than  $5 \times 10^7 \text{ s}^{-1}$ .

#### 4. Discussion

Predissociation of excited states of diatomic molecules may be classified as a *rotational predissocia-*

*tion* or an *electronic predissociation* [22,28]. In the first case only a single electronic state is involved and its potential becomes quasi-repulsive at high  $J$ -levels because of a centrifugal contribution. We have not found evidence of rotational predissociation mechanisms in the states of CO under investigation. In case of electronic predissociation a bound state is partly mixed with another electronic state that is repulsive. There is also a possibility that a bound state couples to another bound state, which is in turn predissociated. Such a situation generally leads to an accidental predissociation. In the following some mechanisms causing predissociation will be discussed, with an emphasis on perturbations of an electrostatic character. So possible spin-orbit interactions with triplet states will not be considered. As repulsive states are not easily identified from spectroscopy ab initio calculations of potential energy curves play an important role in the identification of the dissociation mechanism.

An example of an ab initio calculation, which may be helpful in the interpretation of the present data is that of Cooper and Kirby [24] on the potential curve of the  $W^1\Pi$  state. This is the third  $^1\Pi$  state, after the  $A^1\Pi$  and the  $E^1\Pi$  states. Cooper and Kirby report a double minimum potential for the  $W^1\Pi$  state, with minima at 1.26 and 1.87 Å. In between at 1.57 Å a potential barrier of height  $9395 \text{ cm}^{-1}$  above the lowest minimum exists. At large internuclear distances the double potential correlates adiabatically to the  $C(^1D) + O(^1D)$  dissociation limit. The corresponding dissociation energy is larger than the energy of the local maximum at 1.57 Å. The predissociation behaviour presently observed for  $v=0$  and  $v=2$  states is completely different, in that the predissociation is parity dependent for  $v=0$ , whereas it is parity independent for  $v=2$ . The fact that the predissociation rates of  $W^1\Pi$ ,  $v=0$   $\Pi_e$  states are proportional to  $J(J+1)$ , as well as the fact that the rates for  $\Pi_f$  states are constant at a low level, may be attributed to an electronic coupling to some repulsive  $^1\Sigma^+$  state (see below). This mechanism is unrelated to the form of the double well. For the  $W^1\Pi$ ,  $v=2$  state the situation is different. All rotational levels have an energy just above the second potential minimum at 1.87 Å. The wavefunction therefore spreads out into the outer region, with a density related to the tunneling probability through the potential barrier. This effect is par-

Table 19

Observed and calculated line positions (in  $\text{cm}^{-1}$ ) of the  $W(3\sigma) \ ^1\Pi, \nu=0-X \ ^1\Sigma^+, \nu=0$  transition {28} of  $^{12}\text{C}^{16}\text{O}$  at  $\lambda=97.27$  nm

| $J$ | $R(J)$    | Obs. – calc. | $Q(J)$                   | Obs. – calc. | $P(J)$    | Obs. – calc. |
|-----|-----------|--------------|--------------------------|--------------|-----------|--------------|
| 0   | 102809.83 | –0.03        |                          |              |           |              |
| 1   | 102812.28 | 0.01         | 102805.99                | –0.03        |           |              |
| 2   | 102813.91 | –0.05        | 102804.55                | –0.03        | 102798.29 | –0.04        |
| 3   |           |              | 102802.41                | –0.01        | 102793.04 | –0.01        |
| 4   | 102814.96 | –0.17        | 102799.54                | 0.01         |           |              |
| 5   |           |              | 102795.94                | 0.04         |           |              |
| 6   |           |              | 102791.58                | 0.05         | 102772.93 | 0.09         |
| 7   |           |              | 102786.44                | 0.04         | 102764.63 | 0.00         |
| 8   |           |              | 102780.52                | 0.02         | 102755.72 | 0.07         |
| 9   |           |              | 102773.87                | 0.05         | 102745.98 | 0.07         |
| 10  |           |              | 102766.33                | 0.00         | 102735.40 | 0.01         |
| 11  |           |              | 102758.04                | 0.02         | 102723.88 | –0.18        |
| 12  |           |              | 102748.88                | 0.02         | 102711.94 | 0.02         |
| 13  |           |              | 102738.78                | –0.06        |           |              |
| 14  |           |              | 102727.86                | –0.08        |           |              |
| 15  |           |              | 102716.08                | –0.03        |           |              |
| 16  |           |              | 102703.44                | 0.09         |           |              |
| 17  |           |              | 102689.78 <sup>(a)</sup> | 0.18         |           |              |
| 18  |           |              | 102675.38 <sup>(a)</sup> | 0.53         |           |              |
| 19  |           |              | 102660.08 <sup>(a)</sup> | 1.02         |           |              |
| 20  |           |              | 102644.11 <sup>(a)</sup> | 1.91         |           |              |
| 21  |           |              | 102627.49 <sup>(a)</sup> | 3.27         |           |              |
| 22  |           |              | 102611.01 <sup>(a)</sup> | 5.93         |           |              |

Table 20

Observed and calculated line positions (in  $\text{cm}^{-1}$ ) of the  $W(3\sigma) \ ^1\Pi, \nu=0-X \ ^1\Sigma^+, \nu=0$  transition {28} of  $^{13}\text{C}^{16}\text{O}$  at  $\lambda=97.30$  nm

| $J$ | $R(J)$    | Obs. – calc. | $Q(J)$    | Obs. – calc. | $P(J)$    | Obs. – calc. |
|-----|-----------|--------------|-----------|--------------|-----------|--------------|
| 0   | 102778.72 | –0.06        |           |              |           |              |
| 1   | 102781.08 | –0.03        | 102775.01 | –0.09        |           |              |
| 2   | 102782.77 | –0.00        | 102773.71 | –0.04        | 102767.74 | –0.01        |
| 3   | 102783.81 | 0.06         | 102771.76 | 0.03         | 102762.71 | –0.02        |
| 4   |           |              | 102769.07 | 0.05         |           |              |
| 5   |           |              | 102765.72 | 0.10         |           |              |
| 6   |           |              | 102761.57 | 0.06         | 102743.56 | –0.05        |
| 7   |           |              | 102756.78 | 0.09         | 102735.80 | –0.05        |
| 8   |           |              | 102751.16 | 0.01         | 102727.42 | 0.04         |
| 9   |           |              | 102744.87 | 0.02         | 102718.15 | –0.04        |
| 10  |           |              | 102737.82 | 0.02         | 102708.28 | 0.03         |
| 11  |           |              | 102729.93 | –0.03        | 102697.57 | 0.01         |
| 12  |           |              | 102721.30 | –0.02        |           |              |
| 13  |           |              | 102711.87 | 0.02         |           |              |
| 14  |           |              | 102701.46 | –0.06        |           |              |
| 15  |           |              | 102690.23 | –0.08        |           |              |
| 16  |           |              | 102678.12 | –0.07        |           |              |
| 17  |           |              | 102665.26 | 0.13         |           |              |

Table 21

Observed and calculated line positions (in  $\text{cm}^{-1}$ ) of the  $W(3\sigma) {}^1\Pi, v=0-X {}^1\Sigma^+, v=0$  transition {28} of  ${}^{13}\text{C}^{18}\text{O}$  at  $\lambda=97.33$  nm. Lines marked with (b) are blended

| $J$ | $R(J)$       | Obs. – calc. | $Q(J)$                  | Obs. – calc. | $P(J)$    | Obs. – calc. |
|-----|--------------|--------------|-------------------------|--------------|-----------|--------------|
| 0   | 102746.18    | 0.06         |                         |              |           |              |
| 1   | 102748.27(b) | -0.09        | 102742.62               | -0.01        |           |              |
| 2   | 102749.95(b) | -0.01        | 102741.39               | 0.02         | 102735.73 | 0.08         |
| 3   | 102751.04(b) | 0.11         | 102739.49               | 0.03         | 102730.80 | -0.10        |
| 4   | 102751.04(b) | -0.20        | 102736.96               | 0.04         | 102725.37 | -0.15        |
| 5   | 102751.04(b) | 0.16         | 102733.72               | 0.01         | 102719.44 | -0.05        |
| 6   | 102749.95(b) | 0.10         | 102729.86               | 0.02         | 102712.91 | 0.09         |
| 7   | 102748.27(b) | 0.15         | 102725.38               | 0.09         | 102705.46 | 0.03         |
| 8   | 102745.50    | -0.17        | 102720.04               | 0.00         | 102697.63 | -0.06        |
| 9   |              |              | 102714.14               | 0.07         | 102688.72 | 0.02         |
| 10  |              |              | 102707.33               | -0.02        | 102679.98 | -0.07        |
| 11  |              |              | 102699.87               | -0.00        | 102669.40 | 0.05         |
| 12  |              |              | 102691.50               | -0.10        |           |              |
| 13  |              |              | 102682.49               | -0.02        |           |              |
| 14  |              |              | 102672.60               | 0.04         |           |              |
| 15  |              |              | 102661.67               | -0.05        |           |              |
| 16  |              |              | 102650.00               | 0.04         |           |              |
| 17  |              |              | 102637.45 <sup>a)</sup> | 0.22         |           |              |
| 18  |              |              | 102623.98 <sup>a)</sup> | 0.49         |           |              |

<sup>a)</sup> Lines not included in the fit.

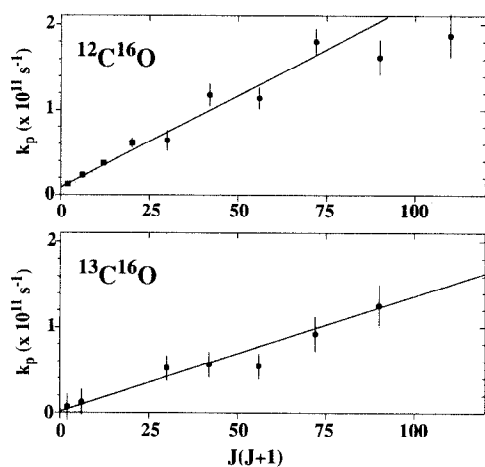


Fig. 18. Rotational-state-dependent predissociation rates for the  $\Pi_e$  components of the  $(3\sigma)W {}^1\Pi, v=0$  state as a function of  $J(J+1)$  for  ${}^{12}\text{C}^{16}\text{O}$  and  ${}^{13}\text{C}^{16}\text{O}$ . Data points for  $J \leq 4$  (■) of  ${}^{12}\text{C}^{16}\text{O}$  were taken from ref. [8].

ity independent. Because eigenstates in the outer well are bound, this tunneling effect in itself cannot explain any dissociation features. However the calculations show [24] that at  $1.72 \text{ \AA}$ , in the adiabatic limit

an avoided crossing of the  $W {}^1\Pi$  and  $E {}^1\Pi$  states occurs. This  $E {}^1\Pi$  state at large internuclear distances correlates to  $\text{C}({}^3\text{P}) + \text{O}({}^3\text{P})$  ground state atoms, lower in energy than the levels of  $W {}^1\Pi, v=2$ . The avoided crossing occurs at approximately  $4000 \text{ cm}^{-1}$  above the lower minimum of the  $W {}^1\Pi$  potential in the range of the higher rotational levels of  $W {}^1\Pi, v=2$ . If a coupling between  $W {}^1\Pi$  and  $E {}^1\Pi$  states is assumed, the wavefunction overlap will therefore be largest for the  $v=2$  level of  $W {}^1\Pi$ . Via this indirect mechanism effective dissociation of  $W {}^1\Pi, v=2$  may take place. Such a mechanism will be parity independent as the potentials hold for both  $\Pi_e$  and  $\Pi_f$  components.

This reasoning raises the question of the rotational and isotope dependence of the predissociation of  $W {}^1\Pi, v=2$  as well as that of  $W {}^1\Pi, v=1$  and 3. The tunneling process through the potential barrier will certainly favor predissociation of the lighter isotope and, because of their centrifugal energy, the higher rotational levels. But the coupling of  $W {}^1\Pi$  and  $E {}^1\Pi$  states sensitively depends on the precise location of the  $W {}^1\Pi$ – $E {}^1\Pi$  potential crossing on the energy scale. So a delicate interplay of these processes will exist and

more detailed information on the potential energy curves is required for a quantitative analysis of this scheme. The  $W^1\Pi, v=1$  state lies below the outer minimum, and consequently the proposed mechanism is not applicable. The rather strong predissociation rate observed by Eidelsberg and Rostas [3] may be due to some electronic coupling, possibly the same that induces the predissociation of the  $W^1\Pi, v=0$  state, but with a larger vibrational overlap factor. The  $W^1\Pi, v=3$  state also strongly predissociates [3]. Here the presently proposed mechanism involving the  $E^1\Pi$  state may play a role. Measurements of parity dependent predissociation in  $W^1\Pi, v=1$  and 3 states may provide definite answers.

Two  $^1\Sigma^+$  states exist that correlate to separated  $C(^3P)$  and  $O(^3P)$  ground state atoms, one being the CO molecular ground state  $X^1\Sigma^+$ . The other was spectroscopically identified as  $D'^1\Sigma^+$  in a laser-induced fluorescence experiment on extremely hot CO by Wolk and Rich [29]. In ab initio calculations [30] an adiabatic double minimum potential for a  $^1\Sigma^+$  excited state was found, resulting from an avoided crossing between two diabatic potential curves. This complex was identified as  $(3s\sigma)B^1\Sigma^+$  and  $D'^1\Sigma^+$  states by Tchang-Brillet et al. [31]. In a detailed study, based on close-coupling of two diabatic potentials they analyzed the B– $D'$  Rydberg-valence interactions. Resulting perturbations, occurring in the form of shifts of level positions, anomalous band intensities and predissociation of the B-state levels could be satisfactorily explained. The inner limb of the  $D'$ -state diabatic potential is found to cross the outer limb of all  $(ns\sigma)^1\Sigma^+$  and  $(np\sigma)^1\Sigma^+$  potentials [31]. Although the  $D'$  state is a weakly bound state, for Rydberg states with  $n \geq 4$ , lying in the range above  $100000 \text{ cm}^{-1}$  only the repulsive inner limb is of interest. Here the  $D'$  state may be regarded as a purely repulsive state. Apart from the predissociation of  $(3s\sigma)B^1\Sigma^+, v=2$  also the predissociation of  $(3p\sigma)C^1\Sigma^+, v=3$  and 4 and the  $(ns\sigma)^1\Sigma^+$  states was attributed to this repulsive part of the  $D'$  state by Tchang-Brillet et al. [31]. Furthermore Drabbels et al. [8] attributed the predissociation of the  $(4p\sigma)K^1\Sigma^+, v=0$  states as well as the  $W^1\Pi, v=0$  and  $L^1\Pi, v=0$  states to this  $D'$  state.

An electrostatic perturbation between two states of  $^1\Sigma^+$  symmetry is homogeneous and has  $J$ -independent interaction matrix elements. Perturbation ma-

trix elements between  $^1\Pi$  and  $^1\Sigma^+$  states will only affect  $\Pi_e$  components and will scale as  $\sqrt{J(J+1)}$ . When the  $^1\Sigma^+$  perturber state in the latter case is purely repulsive, predissociation rates will be simply proportional to the square of the matrix element, so to  $J(J+1)$ , without any resonant features. For the  $W^1\Pi, v=0$  and  $L^1\Pi, v=0$  states such a scaling of the predissociation with  $J(J+1)$  of the  $\Pi_e$  components was observed. This effect, also reported by Drabbels et al. [8] for  $J \leq 4$ , is now confirmed up to higher  $J$ -values. Alternatively for the  $(4p\sigma)K^1\Sigma^+, v=0$  state of  $^{12}C^{16}O$  a rotational-state-independent predissociation rate is presently confirmed up to  $J=20$ . A coupling between  $K^1\Sigma^+$  and  $D'^1\Sigma^+$  will indeed give rise to a homogeneous perturbation with  $J$ -independent matrix elements. For the  $n=6$  term of the  $(np\sigma)^1\Sigma^+, v=0$  Rydberg series it was postulated (see section 3.1) that the predissociation, if occurring at all, is  $J$ -independent, as in the case of the  $n=4$  term. The predissociation of these states can be explained by a coupling with the  $D'$  state. The  $n=5$  term of  $(np\sigma)^1\Sigma^+, v=0$  may well predissociate by an interaction with the  $D'$  state as well at a rate of  $k_p = 2 \times 10^{10} \text{ s}^{-1}$ , similar to  $n=4$  [8]. But we observe an additional, rotational-dependent and stronger predissociation effect, which cannot be attributed to a coupling with the  $D'$  state. Apparently a heterogeneous perturbation with a yet to be identified  $\Pi$  state may cause this effect.

A large number of accidental predissociations were found in the present study that must have an origin in electronic coupling with bound states. From the analysis of the  $^1\Pi, v=2$  state {13} even the spectroscopic constants of an unknown perturber manifold could be deduced from observations. The data are, however, not sufficiently accurate to determine a homogeneous or heterogeneous character of the perturbation. But nevertheless it follows that a state with a band origin at  $\nu_0 = 107708 \pm 2 \text{ cm}^{-1}$  causes the accidental predissociation effect near  $J=8$  in  $^1\Pi, v=2$ .

The  $(4d\sigma)^1\Sigma^+, v=0$  state is exemplary in that it shows how the perturbing matrix element simultaneously causes level shifts and predissociation. Strong accidental predissociation is found at  $J=8, 12$  and 22 and another weak accidental predissociation is found at  $J=19$ . Because the rotational levels of a perturbed and a perturber state can only cross near a particular  $J$ -value, there must be four bound states interacting with the observed  $(4d\sigma)^1\Sigma^+, v=0$  state.

It is possible that a triplet state crossing at three different  $J$ -levels induces these perturbations.

The deperturbation analysis of the  $K^1\Sigma^+$ ,  $v=0$  state of  $^{13}\text{C}^{18}\text{O}$  could be performed with high accuracy, so that even the character of the perturbation could be identified (heterogeneous) as well as molecular parameters of the perturber state derived. The perturber at  $\nu_0=103073.44\text{ cm}^{-1}$  is tentatively identified as the  $E^1\Pi$ ,  $v=5$  state. For more details on this specific case we refer to Eikema et al. [23].

Other accidental predissociations have been identified as well (see section 3). Obviously, as these perturbations are related to bound states, the perturbers will correlate to higher lying potentials for which no detailed ab initio calculations are available yet. Identification of the perturbations in terms of electronic coupling will await future calculations as well as further experimental investigation of the high-lying states of CO.

## 5. Conclusion

In the present investigation a high resolution extreme ultraviolet laser source has been employed for the collection of a large number of data on the excited states of CO in the wavelength range 91–97 nm. Accurate absolute transition frequencies in the XUV have been determined by calibration against the  $I_2$  standard in the visible. Predissociation effects were observed that depend on the particular rovibronic state, parity component and isotopic combination. Error margins on the present values for the predissociation rates are generally 20%. The additional information extracted from the observed relative line intensities in 1 XUV + 1 UV photoionization (see Appendix) provided a consistency check on relative values for the predissociation rates. The dynamic range for the derivation of predissociation rates from linewidth analyses using our XUV laser source is rather limited: reliable values can only be obtained over one order of magnitude in between  $3 \times 10^{10}$  and  $3 \times 10^{11}\text{ s}^{-1}$ . In case of too rapid predissociation the intensities of the 1+1 photoionization signals decrease below the noise level and consequently no resonance features are discernable. At linewidths of  $1.5\text{ cm}^{-1}$  the rotational band structure tends to wash out as is observed in bands {15A} and {15B}. In such cases

study of line broadening of individual rotational components is no longer possible. The lower limit is determined by the instrumental linewidth. The predissociation rates of most of the excited states of CO in the range 91–100 nm lie within the accessible dynamic range.

The present work was partly motivated by questions of astrophysical origin, namely those related to the photophysics of carbon monoxide, which is known to govern the chemical dynamics in large parts of the universe. It is beyond the scope of this detailed spectroscopic investigation to pursue an implementation of results into these photochemical models. The dynamical information in terms of predissociation rates and the spectroscopic information in terms of absolute transition frequencies are definitely more accurate than in all previous nonlaser based studies in the extreme ultraviolet. Drawbacks of the use of our XUV laser setup in combination with 1+1 photoionization are that not all the states identified by Letzelter et al. [2] could be observed and that it is not possible to measure absorption cross sections. Recently accurate values for absorption cross sections were obtained from synchrotron studies by Stark et al. [9,32] on several states of CO.

Although for the modelling of the cold interstellar medium data for  $J \leq 5$  would suffice spectra were analyzed up to much higher values of  $J$ . Such data of high  $J$ -values may have relevance for the modelling of higher-temperature regions, such as e.g. circumstellar envelopes or the thermosphere of Venus [33].

## Acknowledgement

Financial support from the Foundation for Fundamental Research on Matter (FOM) and the Netherlands Organization for the Advancement of Research (NWO) is gratefully acknowledged.

## Appendix. Rate-equation model for the intensities in 1+1 two-photon ionization

A model is presented to calculate the relative spectral line intensities in 1+1 two-photon ionization processes, in case of a rapidly dissociating intermediate state. A level diagram as in fig. 19 is assumed

with a ground state population  $N_1$  and an excited state population  $N_2$ . The ground state is depopulated with an absorption rate  $k_{\text{abs}}$  proportional to the intensity of the resonant laser  $I_{\text{XUV}}$ . The excited state population  $N_2$  is ionized with a rate  $k_{\text{ion}}$ , proportional to the second ionizing field  $I_{\text{UV}}$ . The excited state may also be depopulated by fluorescence rate  $k_f$  and a predissociation rate  $k_{\text{pred}}$ .

Under conditions of “broadband excitation”, i.e. the bandwidth of the laser radiation exceeding the natural width of the transition, populations may be calculated in a rate-equation model. The rate equations are

$$\frac{dN_2}{dt} = k_{\text{abs}}N_1 - k_t N_2 \quad (\text{A.1})$$

and

$$\frac{dN_1}{dt} = -k_{\text{abs}}N_1, \quad (\text{A.2})$$

where  $k_t$  is the total deexcitation rate of the excited level:

$$k_t = k_{\text{pred}} + k_{\text{ion}} + k_f. \quad (\text{A.3})$$

A solution to eq. (A.2) is

$$N_1(t) = N_1^0 \exp(-k_{\text{abs}}t). \quad (\text{A.4})$$

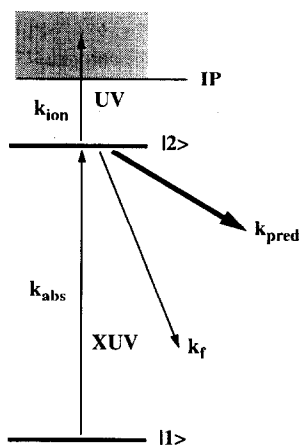


Fig. 19. Generalized level scheme for a 1 XUV + 1 UV photoionization process. Rotational ground state levels  $|1\rangle$  are resonantly excited by XUV radiation. Excited levels  $|2\rangle$  are either ionized by the UV radiation, decay radiatively or predissociate. The latter channel is dominant for the states in CO presently investigated.

This equation holds for the case of non-saturation. Under the condition that  $k_{\text{abs}} \ll k_t$  saturation will not occur, as the population  $N_2$  of the excited state remains low. Insertion of solution (A.4) into the rate equation (A.1) yields

$$\frac{dN_2}{dt} + k_t N_2 = k_{\text{abs}} N_1^0 \exp(-k_{\text{abs}}t), \quad (\text{A.5})$$

where  $N_1^0$  is the ground state population at  $t=0$ . With the boundary conditions  $N_2(t) = 0$  for  $t=0$  and  $t \rightarrow \infty$  the solution to this equation is

$$N_2(t) = \frac{k_{\text{abs}} N_1^0}{k_t - k_{\text{abs}}} [\exp(-k_{\text{abs}}t) - \exp(-k_t t)]. \quad (\text{A.6})$$

Ions are produced during the time of the laser pulse  $T_p$ , in which excited state population is transferred into the continuum with a rate  $k_{\text{ion}}$ . So the ion yield is

$$I_{\text{ion}} = \int_0^{T_p} k_{\text{ion}} N_2(t) dt. \quad (\text{A.7})$$

Inserting the solution for  $N_2(t)$  then gives

$$I_{\text{ion}} = \frac{k_{\text{ion}} k_{\text{abs}}}{k_t - k_{\text{abs}}} N_1^0 \left( \frac{1 - \exp(-k_{\text{abs}} T_p)}{k_{\text{abs}}} + \frac{\exp(-k_t T_p) - 1}{k_t} \right). \quad (\text{A.8})$$

At this point some further assumptions will be made. The absorbing transition is far from saturation, so the exponential containing the absorption rate may be linearized. Furthermore in the present experiment use is made of nanosecond pulsed lasers, so  $T_p \approx 10^{-9}$  s, while the deexcitation of the excited state is fast, i.e.  $k_t \approx 10^{11}$  s $^{-1}$ . The second term in between brackets is then found to be proportional to  $1/k_t$ . Eq. (A.8) then contains two terms: one proportional to  $T_p$  (on the order of  $10^{-9}$ ) and one proportional to  $1/k_t$  (on the order of  $10^{-11}$ ). As the latter term is much smaller it is neglected. With these assumptions eq. (A.8) reduces to

$$I_{\text{ion}} = \frac{k_{\text{ion}} k_{\text{abs}}}{k_t} N_1^0 T_p. \quad (\text{A.9})$$

Here  $k_t$  represents the total depletion of the excited state, including the “natural” decay pathways of fluorescence and predissociation and the forced ionization by the driving field  $I_{UV}$ . Under the conditions of the present experiment with non-focused laser beams (interaction diameter of 1 cm) the ionization depletion is only a minor effect. The excited-state natural lifetime is defined as

$$\tau = \frac{1}{k_{\text{pred}} + k_f}. \quad (\text{A.10})$$

In the case of the highly excited states of CO the predissociation efficiency is larger than 99% and the fluorescence rate is negligible. As long as this holds eq. (A.9) reduces to

$$I_{\text{ion}} \propto \frac{N_1^0 k_{\text{ion}} k_{\text{abs}}}{k_{\text{pred}}} = N_1^0 k_{\text{ion}} k_{\text{abs}} \tau. \quad (\text{A.11})$$

Thus we find that the signal peak intensity is proportional to the excited-state lifetime. We note that  $k_{\text{abs}}$  contains the rotational linestrengths or Hönl-London factors.

The validity of eq. (A.11) is limited by the applicability of the rate-equation model itself. When the laser bandwidth is smaller than the natural width of the transition coherence effects come into play and the time evolution of the populations is governed by the optical Bloch equations [34]. In case of a rapidly predissociating state, excited by laser light with a narrower bandwidth than the natural width, populations were calculated by Ubachs et al. [35]. In the limit

$$\delta\nu_{\text{Laser}} \ll \Gamma = \frac{1}{2\pi\tau c}, \quad (\text{A.12})$$

with the laser bandwidth  $\delta\nu_{\text{Laser}}$  in  $\text{cm}^{-1}$ , the excited state population  $N_2$  was found to be proportional to  $\tau^2$ . The analysis of ref. [35] was performed for continuous wave excitation. The excitation with nanosecond pulses may also be considered quasi-stationary, as long as molecular relaxation mechanisms occur on faster time scales. So under the condition of eq. (A.12) the following proportionality relation is found:

$$I_{\text{signal}} \propto \tau^2. \quad (\text{A.13})$$

In the present experiment a laser is used with a bandwidth in the range  $\Delta\nu_{\text{Laser}} = 0.30\text{--}0.44 \text{ cm}^{-1}$ . Life-

time broadening effects are deduced in the range  $\Gamma = 0.15\text{--}2.0 \text{ cm}^{-1}$ . So for the broadest features the signal is proportional to  $\tau^2$ , whereas for the narrowest lines the observed signals are proportional to  $\tau$ . In the intermediate regime, where  $\delta\nu_{\text{Laser}}$  is about equal to  $\Gamma$ , an intricate relation holds:  $I_{\text{signal}} \propto \tau^\alpha$ , with  $1 < \alpha < 2$  and  $\alpha$  a function of  $(\delta\nu_{\text{Laser}}/\Gamma)$ .

## References

- [1] H. Abgrall, E. Roueff, F. Launay, J.-Y. Roncin and J.L. Subtil, *J. Mol. Spectry.* 157 (1993) 512.
- [2] C. Letzelter, M. Eidelsberg, F. Rostas, J. Breton and B. Thieblemont, *Chem. Phys.* 114 (1987) 273.
- [3] M. Eidelsberg and F. Rostas, *Astron. Astrophys.* 235 (1990) 472.
- [4] M. Eidelsberg, J. Benayoun, Y. Viala and F. Rostas, *Astron. Astrophys. Suppl. Series* 90 (1991) 235.
- [5] G. Stark, K. Yoshino, P.L. Smith, K. Ito and W. Parkinson, *Astrophys. J.* 369 (1991) 574.
- [6] P.F. Levelt, W. Ubachs and W. Hogervorst, *J. Phys. II* 2 (1992) 801.
- [7] P.F. Levelt, W. Ubachs and W. Hogervorst, *J. Chem. Phys.* 97 (1992) 7160.
- [8] M. Drabbels, J. Heinze, J.J. ter Meulen and W.L. Meerts, *J. Chem. Phys.* 99 (1993) 5701.
- [9] G. Stark, K. Yoshino, P.L. Smith, J.R. Esmond, K. Ito and M. Stevens, *Astrophys. J.* 410 (1993) 837.
- [10] E.F. van Dishoeck and J.H. Black, *Astrophys. J.* 334 (1988) 771.
- [11] W.D. Langer, T.E. Graedel, M.A. Frerking and P.B. Armentrout, *Astrophys. J.* 277 (1984) 581.
- [12] Y.P. Viala, C. Letzelter, M. Eidelsberg and F. Rostas, *Astron. Astrophys.* 193 (1988) 265.
- [13] S.S. Prasad and S.P. Tarafdar, *Astrophys. J.* 267 (1983) 603.
- [14] T.G. Philips and P.J. Huggins, *Astrophys. J.* 251 (1981) 533.
- [15] R. Gredel, S. Lepp and A. Dalgarno, *Astrophys. J.* 323 (1987) L137.
- [16] T. Bally and W.D. Langer, *Astrophys. J.* 255 (1982) 143.
- [17] W. Ubachs, K.S.E. Eikema and W. Hogervorst, *Appl. Phys. B* 57 (1993) 411.
- [18] S. Gerstenkorn and P. Luc, *Atlas du spectre d'absorption de la molécule de l'iode entre 14800–20000  $\text{cm}^{-1}$*  (CNRS, Paris, 1978).
- [19] S. Gerstenkorn and P. Luc, *Rev. Phys. Appl. (Paris)* 14 (1979) 791.
- [20] S.N. Dobryakov and Y.S. Lebedev, *Soviet Phys. Dokl.* 13 (1969) 873.
- [21] G. Guelachvili, D. de Villeneuve, R. Farrenq, W. Urban and J. Verges, *J. Mol. Spectry.* 98 (1983) 64.
- [22] H. Lefebvre-Brion and R.W. Field, *Perturbations in the spectra of diatomic molecules* (Academic Press, Orlando, 1986).

- [23] K.S.E. Eikema, W. Hogervorst and W. Ubachs, *J. Mol. Spectry.* 163 (1993) 19.
- [24] D.L. Cooper and K. Kirby, *Chem. Phys. Letters* 152 (1988) 393.
- [25] S. Sekine, T. Masaki, Y. Adachi and C. Hirose, *J. Chem. Phys.* 89 (1988) 3951.
- [26] M. Eidelsberg, J. Benayoun, Y. Viala, F. Rostas, P.L. Smith, K. Yoshino, G. Stark and C.A. Shettle, *Astron. Astrophys.* 265 (1992) 839.
- [27] S. Sekine, S. Iwata and C. Hirose, *Chem. Phys. Letters* 180 (1991) 173.
- [28] G. Herzberg, *Molecular spectra and molecular structure. Vol. I. Spectra of diatomic molecules* (Van Nostrand, New York, 1950).
- [29] G.L. Wolk and J.W. Rich, *J. Chem. Phys.* 79 (1983) 12.
- [30] D.L. Cooper and K. Kirby, *J. Chem. Phys.* 87 (1987) 424.
- [31] W.-Ü.L. Tchang-Brillet, P.S. Julienne, J.-M. Robbe, C. Letzelter and F. Rostas, *J. Chem. Phys.* 96 (1992) 6735.
- [32] G. Stark, P.L. Smith, K. Ito and K. Yoshino, *Astrophys. J.* 395 (1992) 705.
- [33] J.L. Fox and J.H. Black, *Geophys. Res. Letters* 16 (1989) 291.
- [34] R. Loudon, *The quantum theory of light* (Oxford Science Publishers, Oxford, 1990).
- [35] W. Ubachs, G. Meijer, J.J. ter Meulen and A. Dymanus, *J. Chem. Phys.* 84 (1986) 3032.